A new mouse model of bone breast cancer metastasis to study the anti-metastatic efficacy of monocyte-mediated delivery of IFNα

Student: Moustafa Sherif, 43365694

Supervisor: Dr. Roberta Mazzieri

Location: Translational Research Institute (TRI), University of Queensland Diamantina Institute (UQDI)

Course: Advanced Research Project & Seminar (BIOC7022), School of Chemistry and Molecular Biosciences (SCMB), Faculty of science

Program: Master of Molecular Biology (Advanced) (MMolBiol (Adv) #32)

Contents

I. Abstract

The tumor immunosuppressive microenvironment is the main challenge to cancer immunotherapy efficacy. By transducing HSCs with a Tie2-interferon-alpha (IFNα) transgene, we converted a tumor homing monocyte subpopulation characterized by the expression of the Tie2 receptor (TIE2-expressing macrophages: TEMs) into an effective tumor-targeted delivery vehicle for this potent immune-stimulatory molecule. This approach intensely repressed both primary and lung metastatic breast cancers in mouse and human hematochimeric models. Because Type I IFN silencing has a key role in maintaining breast cancer bone metastasis, we hypothesized that our IFNα delivery approach could efficiently inhibit this lethal form of breast cancer. Toward this goal we established new tumor cell lines (4T1.2sLuc) that steadily secrete Gaussia Luciferase (sGluc) in the blood and urine to facilitate the longitudinal measurement of total metastatic burden over time. The sGluc was detected in the blood of tumor bearing mice for the first few days, but quickly dropped down despite a normal tumor growth. Further investigation is required to determine the mechanism responsible for the observed decrease in sGluc signal.

Moreover, with the final goal of investigating whether adoptive transfer of genetically engineered monocytes could be considered as an alternative to HSCs transplantation for the delivery of IFNα, we are developing efficient isolation protocols for adult monocytes. We identified the spleen of tumor bearing mice as a rich source of donor monocytes. However, further optimization of the isolation protocol is required. Finally, preliminary data suggest that adoptively transferred mature monocytes are able to home to primary mammary tumors and develop into macrophages.

II. Introduction

Breast Cancer. Breast cancer is the most frequent malignant tumor and second leading cause of cancer death among women in western communities (1) including Australia. On top of the physical distress on patients, there is substantial emotional stress for these patients and their relatives. The patient has to psychologically tackle with multiple anxieties during diagnosis and treatment of the disease, like coping with therapies costs, day-care and work burdens (2). The microarray-based gene expression profiling based on massive parallel gene expression analysis and immunohistochemistry, have been incorporated into clinical practice to categorize the different types of breast cancer at the transcriptomic and molecular levels into two major groups of estrogen-receptor (ER)-positive and ER-negative breast cancers (3). In each group, there are additional molecular subtypes that represent unrelated diseases affecting the same anatomical location (4). Among those subtypes, the most invasive form of breast cancer is classified as invasive ductal carcinoma not otherwise specified (IDC NOS). Despite this molecular classification, the decision-making for the existing treatment is fundamentally based on the clinicopathological markers (HER2+, basal-like, luminal) (5) and genetic testing to determine the best type of adjuvant (6).

Current treatment strategies. Breast cancer treatment often includes a combination of systemic interventions (immunotherapy agents, hormonal maneuvers, chemotherapy, and targeted therapy) and local treatments (radiotherapy, surgery) (7). Current chemotherapy such as bisphosphonates can lessen the symptoms, but is hardly ever curative (8) and sometimes toxic mainly because its generic targeting both cancer and normal cells which leads to destructive effects in normal tissues such as brain cognitive deficits (9). Because breast cancer metastasis is a key factor for long-term patient survival, the biologists were inspired to investigate the genetic and biological pathways of breast cancer metastasis to characterize

new therapeutic molecular targets. In order to do that, comparable studies between *ex vivo* assays such as microarray analysis and in situ hybridization, and *in vivo* studies using murine tumor models have been valuable to show the genetic patterns that are involved in cancer recurrence and metastatic relapse to different organs (10).

Primary tumor removal dilemma. Removal of the primary tumor is not always a solution because of the fact that the primary tumor is producing angiogenesis inhibitors (11). Therefore, the primary tumor mastectomy resectioning might enhance the growth of micrometastatic foci already disseminated to distant organs. Other studies also claimed that surgery could suppress the cell-mediated immunity which help the tumor cells to regrow (12). In contrary, other reports showed that removal of the primary tumor might prevent its potential risk of being a seed source for the dissemination of new metastases, and increase its sensitivity to chemotherapy (13).

Metastasis: a multistep process. Despite treatments, about 3%–6% of all breast cancer patients including more than 25% of early-stage patients will ultimately develop metastasis. Metastatic breast cancer patients have a much worse prognosis despite the high relative survival rate for breast cancer in general. Only less than 30% metastatic patients have 5-year survival (14). Thus, new therapies for the treatment of the metastatic disease will have a great influence on breast cancer survivorship.

The metastatic cascade encompasses many sequential phases that starts with the primary tumor cells invasion to neighboring tissue before intravasate into the blood circulation or lymphatic system. The tumor cells are then disseminated into distant organs where they undertake cell cycle arrest and attach to blood capillaries (15). Once extravasating into the new organ parenchyma, they will proliferate and secrete proangiogenic cytokines. While adapting to the new microenvironment, metastatic cells seek to survive and grow through

concurrent evasion of the apoptotic signals and the anti-tumor immune reaction. This primary metastatic process never stop and can produce secondary metastases (16, 17).

Genes associated with the metastatic process are non-essential stress response genes that encode extracellular matrix-degrading proteinases, homing receptors and ligands. In cancer cells, multi-subunit transcription factor complexes control the expression of these metastatic genes. These transcription factors are downstream to the oncogenes that triggers specific genetic programs which are important for invasiveness and cell cycling (15).

Bone is one of the most common locations of metastasis in many late malignant tumors. This includes 75 % of breast cancers. Bone metastases leads to activation of osteoblastic bone resorption which causes severe pain, hypercalcemia, joints compression, pathologic fractures, and even death for 80 % of patients in 5 years (18). The osteolytic activity is induced by activation of genes such as macrophage inflammatory protein (MIP)-1α, RANK Ligand (RANKL), IL-3, annexin II, IL-6, TNF-α and MMP9 (19) in the bone microenvironment (20).

Metastatic breast cancer cases represent the majority of breast cancer deaths. Determinant factors affecting metastases embrace the tumor microenvironment, intrinsic tumor cell factors, tumor-specific immune reactions and tumor angiogenesis. Detecting early metastasis might be very determinant to stop further cancer progression. New emerging methods like circulating tumor cells assays are helping in predicting and characterizing early metastasis in patients. However, we still need profound knowledge of the cancer metastatic cascade that would be invaluable for evolving therapies to battle metastasis progression (16).

After mapping several chromosome insertions, deletions, translocations, and mutation in tumor tissues, researchers found two sets of genes that participate in breast cancer metastasis which were classified as metastasis promoting genes such as MEK1 and ras, and suppressor

genes like TIMPs, NME1 and Maspin. Most of metastasis promoting genes are involved in cell adhesion, motility, cell arrest, chemoattraction, as well as, provoking immune cells apoptosis or function modification. The suppressor genes can not only slow primary tumor development, but most importantly limit their metastatic potential. More recently novel Proteomic technologies have helped discovering other posttranslational modifications that cannot be genetically mapped (21). The impact of tumor-associated stromal cells on tumor cells invasion and growth capabilities has been neglected from the entire tumor gene expression analysis. To identify the masked genetic etiology in stromal cells, the cell specific profiling will be the most important tool (22).

Tumor microenvironment different components. Tumor complexity does not depend only on tumor cell heterogeneity, but rely on all the cells infiltrating the tumor microenvironment that form the tumor stroma, including immune cells, tumor associated fibroblast, and the vascular endothelium (23). Such a complexity create a dynamic and evolving cross-talk between the different components of the tumor stroma that strongly affects all steps of tumor progression, including tumor growth, immune escape, and metastasis dissemination. Understanding the cellular and molecular communications that support tumor progression is essential to identify therapeutic targets and prognostic markers for advanced metastatic breast cancer. Among the different types of tumor infiltrating cells, immune cells, and in particular myeloid cells, have been shown to play fundamental roles in promoting tumor progression (24).

Macrophages, TAMs, and MAMs. Macrophages represent the final step of monocyte differentiation upon extravasation and migration into tissues. Macrophages are key innate immune system players with an outstanding capability to identify and engulf pathogens. They can adapt themselves to microenvironmental changes due to their notable plasticity (25). These changes are important not only for their immune activity such as pathogen clearance

and inflammation, but also for their important role in homeostasis during resolution of inflammation, wound healing, as well as, tissue remodeling and development. Depending on the specific signals present in the microenvironment, macrophages can be activated toward a classical M1 phenotype by endogenous/pathogen signals and Th1 cytokines (e.g TNF-α and IFN-ɣ). Alternatively, anti-inflammatory mediators, such as M-CSF, TGF-β, IL-4 and IL-10, stimulate an anti-inflammatory response characterized by an M2-like phenotype (26, 27). These anti-inflammatory macrophages are endowed with immunosuppressive and tissue remodeling activities.

Immune evasion and the establishment of an immunosuppressive microenvironment are known hallmarks of cancer (28). Tumor immune evasion happens through different mechanisms, including a) down-regulation in the expression of tumor-associated antigens and MHC class I molecules, b) altered expression the tumor suppressor genes, oncogenes, and signal transduction pathways (29), and c) secretion of immunosuppressive factors such as transforming growth factor (TGF)-β or interleukin (IL)-10 (29, 30), associated with robust leukocyte infiltration of immunosuppressive myeloid cells, (31), regulatory T cells (Tregs) (32), regulatory/tolerogenic dendritic cells (DCs), and N2 neutrophiles (33) myeloid-derived suppressor cells (MDSCs) to inhibit the anti-tumor immune response, and enhance the neoangiogenesis which is essential for tumorigenesis and metastasis. The heterogeneous myeloid cell population infiltrating a tumor includes dendritic cells (DCs), macrophages and granulocytes (29).

Tumor-associated macrophages (TAMs) density in human breast carcinomas associates with poor prognosis (25). Depletion of macrophages from breast cancer mouse models either by therapeutic or genetic treatments such as in the M-CSF-deficient mice (34), led to inhibition of tumor growth (35) and metastasis (35, 36). TAMs can be divided into two main subpopulations; M1-like inflammatory TAMs and M2-like immunosuppressive and pro-

tumoral TAMs. Pro- and anti-tumoral TAMs are characterized by the differential markers expression of MHC II or CD206, and different VEGF levels (37). Remarkably, M1 and M2 polarization could be modulated. It was recently shown that while GM-CSF inhibit breast cancer tumor progression and metastasis in mice by raising an antitumoral response in TAMs, the M-CSF treatment might help cancer growth by further polarizing them towards an M2 phenotype (38).

M1 and M2 represent two extremes of a continuum including many different sub-populations with specific diverse functions in tumor progression. For example, metastasis-associated macrophages (MAMs) express high level of CCR2 and are responsible for the tumor cells extravasation and therefore the seeding of new metastasis. On the contrary, the inflammatory CD11c+ macrophages express low level of CCR2 (39). Therefore, inhibition of the CC-chemokine ligand 2 (CCL2) CC-chemokine receptor 2 (CCR2) axis could lead to decrease MAMs recruitment and so dramatically decrease the metastatic seeding of breast cancer to the lungs (40).

TEMs-mediated delivery of IFNα. Dr. Mazzieri and her colleagues have identified a subpopulation of monocytes/macrophages characterized by the expression of the Angiopoietin receptor TIE2 (41) (TEMs: TIE2-expressing monocytes/macrophages) and endowed with immunosuppressive and pro-angiogenic activities. TEMs are efficiently recruited to tumors, where they up-regulate Tie2, but are occasionally recruited to normal organs. *In vivo* blockade of the Tie2 ligand Angiopoietin 2 did not hinder TEMs recruitment but inhibited Tie2 upregulation in TEMs, their perivascular localization and their ability to promote angiogenesis. Similarly, Tie2 knockdown in TEMs resulted in loss of TEMs perivascular localization and diminished tumor vascularization (42). TEMs have a gene expression signature characteristic of M2-polarized TAMs that endorse tumor vascularization and promote immunosuppression. Therefore targeting tumor-infiltrating TEMs, will increase

the efficacy of antiangiogenic treatments by countering evasive resistance mediated by pro-angiogenic myeloid cells (43).

Because the expression of Tie2 was found to be three times higher in tumor-derived TEMs than in blood-derived TEMs **(Figure.1A)**, Dr. Mazzieri and colleagues utilized the selective expression of the TIE2 receptor and the tumor homing ability of TEMs to reverse the immunosuppressive microenvironment, by converting them into cellular vehicles for the delivery of IFN-α, a potent anti-tumoral molecule (see below). Hematopoietic stem cells (HSCs) were transduced with the IFN-α transgene downstream to the Tie2 promoter (41). Because Tie2 is also expressed in the HSC compartment and exposure of HSCs to IFNα might interfere with their quiescence, the IFNα transgene expression was silenced in the HSC compartment but preserved in mature monocytes by adding the target sequences for miR-126 and miR-130a (mirT) in the Tie-IFNα lentiviral vector (44) (**Figure.1B).** The microRNAs miR-126 and miR-130a are expressed only in the HSC compartment, and as a consequence they will silence expression of the Tie2-IFNα lentiviral vector in HSCs but not in more differentiated hematopoietic cells, including mature monocytes (45).

(A)

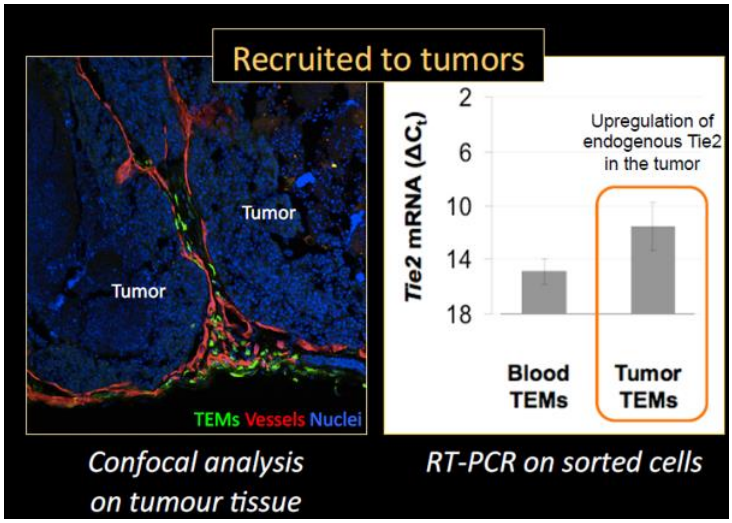

(B)

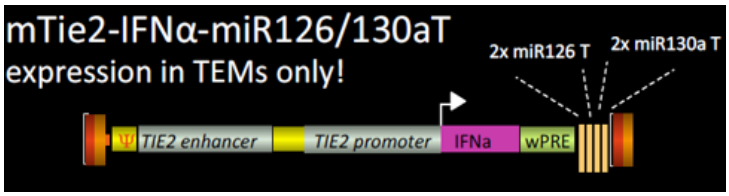

Figure.1: TEMs upregulate Tie-2 expression after homing tumor tissues. **(A) Left:** TEMs (green) and blood vessels (red) immunostaining and nuclear staining (blue) in MMTV-PyMT tumors. **Right:** RT-qPCR measurements of Tie2 transcript in blood-derived Tie2-expressing monocytes (TEMs) and tumor-derived TEMs sorted from FVB/Tie2-GFP mice. This figure was adapted from De Palma et al.(41). **(B)** Murine Tie2-IFNα delivery platform. Post transcriptional regulated vector: miR126 and miR-130a target sequences (mirT) were used for detargeting the IFNα expression from the HSCs compartments. This figure was adapted from Escobar et al. (46)

Interferons. Interferon-α (IFN-α) is an immunoregulatory pleiotropic cytokine with known and diverse anti-tumor activity (22). IFN-α displayed clinical efficacy in the treatment of different kinds of cancer, such as breast carcinoma, chronic myelogenous leukemia, melanoma, orthotopic human gliomas and renal cancer (41). Type I IFNs, including IFNα, not only increase angiostatic molecules and the expression of tumor-suppressor proteins such as p53 (47), but also trigger dendritic cells, NK cells and macrophages, to produce pro-inflammatory cytokines such as IL-15 that increase T cells survival and cytolytic activity (22, 48). Type I interferon signal trough the IFN receptors (IFNAR1 and IFNAR2) and activates the Janus kinase (JAK)–signal transducer and activator of transcription (STAT) pathway, leading to transcription of IFN-stimulated genes (ISGs) (49). Host, pathogen and environmental factors induce type I interferon expression in innate cells.

Blockade of the type I IFN receptor with specific monoclonal antibodies, or using IFNAR1-deficient mice inhibited the ability of the immune system to reject very immunogenic syngeneic sarcomas. These results illustrate the vital role of type I IFNs in mediating tumor rejection response (50). The IFN mediated tumor rejection capacity is mediated by the MHC class I pathway upregulation and enhanced antigen processing and presentation to the adaptive immune system (23).

Interferon clinical toxicity. Despite using IFNα in the treatment of viral and malignant diseases for more than 30 years, its use was drastically reduced over the last decade (51) because of the high toxicity associated with its systemic delivery, such as hematological toxicity on megakaryocytic and erythroid lineages, flu-like symptoms, fatigue, musculoskeletal pain, sullenness, irritability, anxiety, among others. The general inadequate therapeutic efficiency of current anti-tumor type I IFNs based treatments is mainly due our inability to specifically target I type I IFNs to the exact tumor location thereby avoiding excessive systemic toxicity. Other delivery strategies are therefore needed to attain effective and safe IFN delivery in cancer patients. This significant toxicity and ineffectual dosing has motivated Dr. Mazzieri and her colleagues to develop the cell-based and gene-based strategy described above for the targeted delivery of the IFNα to tumors without limiting its efficacy, but reducing the toxicity associated with its systemic delivery. They used TEMs as vehicles for the tumor targeted delivery of IFNα that led to substantial antitumor responses by activating both innate and adaptive immune cells, as well as by inhibiting tumor angiogenesis.

Type I interferon significance in metastasis. Recently, Bidwell et al. (22) have shown that bone metastases incidence is associated with repression of a considerable number of target genes of the interferon regulatory factor 7 (Irf7). This was observed in patients as well as in the 4T1.2 mouse model of breast cancer bone metastasis. Irf7 is widely expressed in 4T1.2

primary tumors, but not in the corresponding bone metastasis. Administration of interferon to restore Irf7 expression in tumor cells inhibited bone metastases. IFN immunotherapy considerably lowered the metastasis to the femur and spine, despite the fact that treatment did not disturb 4T1.2 *in vitro* cell proliferation, *in vivo* primary tumor growth, or even the degree of lung metastasis (22). To show the importance of the IFN signaling in modulating an anti-tumor immune response, mice lacking the IFN receptor or CD8+ T cell and natural killer (NK) were used as recipient mice for the 4T1.2 tumor cells. These experiments demonstrated that the metastasis inhibition induced by the IFN immunotherapy was dependent on IFN signaling to host CD8+ T cell and NK immune cells (22).

IFN anti-tumor activities. The IFN-α sustainable localized production has been categorized as influential angiogenesis inhibitor by directly impairing the endothelial cells (ECs) proliferation and migration. This is mediated by the upregulation of ECs negative regulators (24). Additionally, IFN-α down-regulates vascular endothelial growth factor (VEGF) and IL-8 expression (52), and prevents expression of fibroblast growth factors (FGF) by tumor cells (53). This anti-angiogenic properties are associated with increased hypoxia, ischemic necrosis and consequent tumors regression (24).

Type I IFNs can endorse the innate and adaptive immune functions to produce antitumor effects mostly through acting on the host hematopoietic cells. Type I IFNs activate NK cells that produce IL-15, to prime T cells which increase the production of stromal angiostatic molecules and increase T cells survivability. Additionally, Type I IFNs upregulate the expression of MHCI molecules and activate dendritic cells which increase the cytolytic activity of macrophages (23, 41). Increased infiltration of immune effector cells ($CD8^+$ T cells and NK cells) to tumor tissues was noticed after Type I IFN systemic administration with concomitant reduction of immunosuppressive MDSCs in the bone marrow and blood.

This anti-metastatic immune responses could intensely decrease bone metastasis and protract metastasis-free survival (22) in the 4T1.2 model.

4T1.2 mouse breast cancer cells. Only *in vivo* preclinical models can reproduce the complexity of the tumor-stroma interactions and their relevance to tumorigenesis and metastatic progression. Toward this purpose, the *in vitro* studies using traditional cell culture have become insufficient, with the exemption of emerging new 3D culture models (54) that at least partially simulate the *in vivo* microenvironment. The best *in vivo* immunocompetent models should have tumor and host compatible stroma (55) that reproduce the full breast cancer metastasis course (56), including orthotopic growth of the primary tumor and spontaneous metastasis to other organs relevant to the human breast cancer in the presence of complete functional immune system.

The high similarity between some human cancers and preclinical mouse models is particularly relevant for breast cancer (57). In this research project, we used the mous breast cancer cell line 4T1.2 derived from BALB/cfC3H immunocompetent mice. 4T1.2 mammary carcinoma tumor cells were derived by single cell cloning from the parental 4T1 cell line (58) (**Figure.2**). 4T1.2 cells can be injected into immunocompetent BALB/c mice, thus allowing for the investigation of tumor-host interactions at early phases of primary tumor growth, invasion, and spontaneous metastasis dissemination. Orthotopically injected 4T1.2 cells are very tumorigenic and invasive and spontaneously metastasize via vasogenic and lymphogenous routes to many organs such as lung, axillary lymph nodes, femur, spine, kidney and heart but rarely metastasize to the spleen, brain, and liver (59). The 4T1.2 is ideal for studying bone metastasis because it results in pelvic limb paralysis (57) and high plasma altitudes of parathyroid hormone-related protein (PTHrP) and calcium, which is similar to human cancer hallmarks (60).

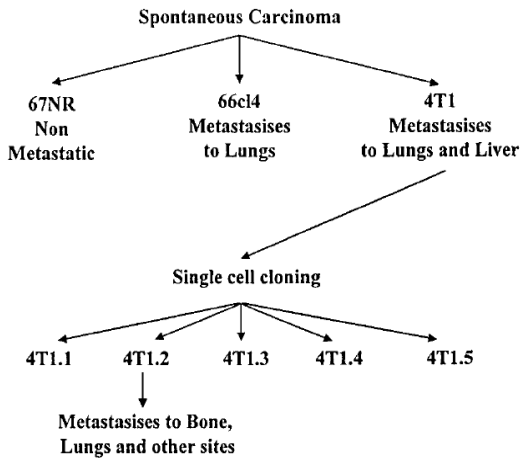

Figure.2: Flow chart adapted from Lelekakis et al.(58) to show the different breast tumor cell metastatic and non-metastatic cell lines. In this study, we used the 4T1.2 cells which were subcloned from the 4T1 parental cell line.

By comparing the highly metastatic 4T1.2 cells with the non-metastatic 67NR and weakly metastatic (168FARN and 66cl4), it was shown that the 4T1.2 metastatic ability depends mainly on their invasive and adhesion capacities and not on their pro-angiogenic and proliferative activities. Q-RT-PCR and microarray analysis showed that genes identified using 4T1.2 model have been identified before in human metastatic breast cancer progression (57). Interestingly, 10% of the 89 metastatic genes in 4T1.2 were encoding ECM molecules that are responsible for the physiological remodeling in the tumor microenvironment, to help the metastatic progression (61).

4T1 cells are triple-negative breast cancer cells that do not express the progesterone receptor (PgR), estrogen receptor (ER), or the epidermal growth factor receptor 2 (HER2). This makes them more aggressive with high possibility for metastasis and recurrence than other breast cancer cell lines with limited therapeutic choices. Thus, 4T1.2 cells will recapitulate the behaviour of human triple negative breast cancer, one of most the aggressive human breast cancer types (60). This, together with the recent data on silencing of Type I interferon

signaling in 4T1.2 bone metastasis (22), identifies this model as the best available model to investigate the efficacy of our IFN-delivery strategy on breast cancer bone metastasis.

4T1 and 4T1.2 tumor cells can also be injected systemically to study the final stages of metastasis dissemination and seeding in different organs. The final target organ in this model of experimental metastasis depends on the injection route, for instance, tail vein injection usually induces lung metastasis, while the intracardiac injection provokes both lungs and bone metastasis (62). Experimental metastasis allow testing of therapeutic strategies in the absence of confounding effects on the primary tumor.

Monitoring metastatic growth. For entirely comprehending the efficiency of our immune therapy to treat breast cancer, it is important to understand how the treatment decrease the metastatic burden in bones and lungs and modulates their distribution within the organs. Molecular imaging is a versatile technique for longitudinal analysis of cellular localization and metastasis. Establishing reporter genes in tumor cells for tracking their localization and proliferation profile is a potent tool for cancer cell biology. The genetic reporter should be expressed optimally and uniformly in the host cells, have a low intrinsic constancy to rapidly mirror the transcriptional dynamics, and evade uncharacteristic expression in case of cryptic regulatory sequences (63).

We aimed to develop a novel bioluminescence assay based on naturally secreted, and very sensitive sGluc that allows monitoring of micrometastasis tumor burden in real-time because it can be detected in the blood of animals *ex vivo*, as well as, conditioned medium of tissue culture cells (64). Towards this goal, 4T1.2 tumor cells, carrying the intracellular Fluc and mCherry reporter genes, were further transduced with a lentiviral vector encoding for sGluc and the CFP reporter gene. For additional precise quantification of metastasis at the end point

of treatments, a real-time quantitative PCR (q-PCR) assay for mCherry reporter was used to measure of tumor burden within metastatic organs.

The use of sGluc to quantify tumor burden was validated by correlating the sGluc signal with that of *in vivo* imaging of the intracellular Fluc, as well as with direct tumor volume measurements and X-ray Faxitron for the mice skeleton. The IVIS platform can cover many high-throughput two-dimensional or tomographic imaging applications with the highest sensitivity levels for bioluminescence such as luciferase, and fluorescence like mCherry proteins by integrating anatomical and functional tools.

Adoptive transfer versus HSCs transplantation. The bone marrow, adult peripheral blood, and foetal umbilical cord can be readily available sources for HSCs that can be easily characterized and transduced for cell-based gene therapies. This helped in removing the need for boost recurrent gene therapy because of the HSCs capacity for self-renewing and differentiation (65). However, the arbitrary insertion of retroviral vectors in the chromosomal DNA of HSCs might result in potentially dangerous and harmful mutations (insertional mutagenesis) that will stay long-term with the patient (66). To overcome this problem, we are now investigating the usefulness of short-life span mature cells such as monocytes as alternative to HSC transplantation. Monocytes have the great advantage of naturally infiltrating all tissues including often unapproachable organs like bones and brain (67).

The recruitment of the monocytes targeted therapy after being adoptively transferred into the tumor tissue is crucial for the analyzing the efficacy of our strategy. The monocytes usually develop into dendritic cells and macrophages after extravasation for the initiation of inflammation immune response against tumor cells and/or infectious micro-organisms (68). Therefore, the noninvasive monocytes/macrophages tracing *in vivo* should help for the better

quantification, visualization, and localization of these cells. For this purpose, to monitor the *in vivo* tumor homing ability of adoptively transferred monocytes, we used a noninvasive Cell Proliferation Dye eFluor® 450 that binds to any cellular proteins containing primary amines. This dye does not disturb monocytes function and viability, and correspondingly dispersed to 7 daughter cell generations that can be analyzed as consecutive halving of the dye fluorescence strength (69). The *in vivo* distribution of adoptively transferred monocytes was analyzed by FACS on isolated organs and tissues.

Hypothesis. Silencing of Interferon-α (IFNα) was illustrated as a critical mechanism that support breast cancer metastasis to bones. In order to deliver this potent immune-stimulatory molecule locally to the tumor tissues, we developed a cell- and gene based therapy able to reverse the immunosuppressive microenvironment of breast cancer. We now hypothesis that this IFNα delivery therapy will intensely inhibit lung and bone breast cancer metastasis.

In order to test this hypothesis, we propose to develop a novel mouse model of bone breast cancer metastasis by generating 4T1.2 cells stably expressing the secreted Gaussia luciferase (sGluc) that allows the longitudinal measurement of metastatic burden in the blood of tumor bearing mice.

Aims. The main objectives are to study the anti-metastatic effects of our TEM-mediated delivery of IFNα we aim to 1) produce a novel tumor cell line (4T1.2sLuc) by lentiviral transduction to the 4T1.2 cell line, 2) test the stable expression of the secreted sGluc *in vitro* in tissue culture medium and *ex vivo* in the blood of tumor bearing mice. This system will allow independent, reliable and real-time monitoring of the tumor growth by analysing the blood *ex vivo*. sGluc levels will be correlated to different *in vivo* and ex-vivo assays such as Fluc IVIS imaging, X-ray Faxitron, and mCherry taqman analysis of the affected organs. Moreover, we aim to perform adoptive transfer of adult monocytes into tumor bearing mice to test their homing capability and explore it as an alternative to HSC transplantation.

III. Materials and methods

4T1.2 mouse breast cancer cells. All cell lines were maintained in RPMI media (Gibco cat. no. 11875) supplemented with 10% FBS, stable glutamine, sodium pyruvate (sigma, cat. no. S8636), and Penicillin Streptomycin (Pen Strep; Gibco cat. no. 15140-122). The cells were incubated in standard cell culture conditions of 5% CO_2 and 37°C.

Lentivirus vector transduction and of 4T1.2 cells and sorting. Two sGluc lentiviral vectors (HA and Flag) were kindly provided by Dr. Lorenzo Bombardelli (The Netherlands Cancer Institute, Amsterdam).

Bacterial transformation for plasmids propagation. The One Shot® TOP10 Chemically Competent Escherichia coli (Invitrogen) were used for propagation of HA and Flag plasmid constructs. The sGluc plasmids with two different tags (HA and Flag) were received on filter papers, and eluted in 100 µl TE buffer (QIAGEN, cat. no. 12362). For each transformation, 2µl of DNA was added to 20 µl of the defrosted bacterial cells and incubated on ice for 15 minutes, followed by heat shock at 42°C for 45 seconds and incubation on ice for 2-3 minutes without shaking. The cells were allowed to recover in 200µl SOC (2% Bacto-Tryptone, 0.5% Bacto-Yeast extract, 10mM NaCl, 2.5mM KCl, 10mM MgCl2, 20mM glucose) broth (Invitrogen, Cat. No. 15544-034) and then incubated for 5 minutes at 37°C. Cells were plated on Luria-Bertani (LB) agar plates containing 100ug/ml ampicillin antibiotic and incubated at 37°C overnight to select the transforming colonies. Only transformed bacteria that uptake the plasmids with ampicillin resistance gene and express beta-lactamase could survive on the agar plates. We then picked up a single colony per plate and transferred it to 3-4 ml of LB broth (1% Bacto-Tryptone, 1% NaCl and 0.5% Bacto-Yeast extract) with shaking (200-250 rpm) for 7-10 hours to increase cell density by cell aeration. The mix was

then was transferred to 250ml LB broth and incubated at 37ºC for overnight with shaking (200 rpm).

Isolation of plasmid DNA from E.coli. The plasmids DNA were isolated in large-scale using PureLink® HiPure Plasmid Maxiprep Kits (Invitrogen, cat. no. K2100-06) as per the manufacturer's protocol. The cells were first resuspended in solution R3 (50 mM Tris-HCl, pH 8.010 mM EDTA) and then lysed with solution L7 (0.2 M NaOH, 1% (w/v) SDS); NaOH denatures genomic and plasmid DNA, while SDS solubilizes cellular proteins after disrupting the lipid membranes. To neutralize the acidic pH, the Precipitation Buffer N3 (3.1 M Potassium acetate, pH 5.5) was added. Potassium acetate precipitates the cellular debris, in consort with SDS from the solution in KDS form. While the plasmid DNA remains in the solution, the chromosomal DNA renatures, tangled and stuck in the precipitate that was then removed by centrifugation. The Plasmid DNA were then purified using equilibrated column and precipitated using isopropanol. The plasmid DNA in the precipitate is washed with 70% ethanol after being pelleted by high speed centrifugation, to remove excess salts and resuspended in TE Buffer. The purified plasmids concentration were measured by Nanodrop; HA plasmid concentration was 5007.1 ng/ul, while Flag plasmid concentration was 4794 ng/ul. The plasmid concentrations were adjusted to 1000 ng/µl and stored at −30°C.

Production of lentiviruses. 2x10^7 293T cells were cultured 8 hours before co-transfection with the following plasmid combination: 9 ug VSV-G envelop plasmid, 12.5ug pCMV.gag/pol and 6.25ug REV packaging plasmids that produce VSVG -pseudotyped retrovirus, 30-35 ug sGluc transfer plasmid (HA or Flag), and 15µl of pADV plasmid. The 125 µl CaCl2 and 1250 µl of 2x HBS were then added before transferring to the cells. The medium was changed 14 hours post-transfection, then the supernatant was collected 30 hours after the medium changed and frozen at -80°C.

Lentiviral transduction by spinduction. 10,000 4T1.2 cells/well were plated overnight before adding 25µl of the lentivirus supernatant and centrifuged the plate at 2500 rpm for 2 hours. The cells were washed in the next day, and replaced with fresh complete media (**Figure.4A).**

Sorting the transduced 4T1.2 cells. We sorted each of the transduced 4T1.2 cell lines two times using FACS**.** In the first sorting (**Figure.4B**) only the cells with high CFP expression were sorted, while in the second sorting (**Figure.4D**) we sorted for those cells with high CFP expression only (single positive) and those with high CFP and mCherry expression (double positive), thus generating four cell lines: HA+ (sGluc+), HA++ (sGluc+ Fluc+), Flag+ (sGluc+), and Flag++ (sGluc+ Fluc+).

Post sorting analysis. We confirmed sGluc and Fluc expression in the transduced 4T1.2 cells using the corresponding CFP and mCherry reporter genes. After the first sorting we used fluorescence microscopy (**Figure.4C)**, and after the second sorting (**Figure.5**) flow cytometry.

***In vitro* bioluminescence luciferase assay.** Sorted and parental cells were plated at decreasing concentrations (1:10 serial dilutions). Conditioned medium and cell extracts were collected 24h later and analyzed for the levels of sGluc (using Promega coelenterazine substrate) and Fluc (using PerkinElmer britelite substrate) respectively. The following validation steps were performed as described.

1. Testing the luciferase machine efficacy in measuring the signals. We measured the efficacy of the automatic injectors of Orion II Microplate Luminometer in quantifying both the Fluc and sGluc signals (**Figure.6**).

A. Fluc. Different ratios of 4T1.2 cell lysate (positives for Fluc only, before sGluc transduction) and parental cell lysate (negative for both luciferase) and of known protein concentrations as measured by Bio-Rad Protein Assay (data not shown) were tested for the levels of Fluc. The luminometer protocol was designed for dual luciferase measurements with 2 seconds delay time in between and 10 seconds for each measurement. Samples were prepared and analyzed as described below.

B. sGluc. The conditioned medium of HA++ 4T1.2 cells was used to measure the variability in microplate readings between the different wells for the same sample in technical triplicates. The triplicates were tested in different ten serial dilutions with PBST (Phosphate Buffered Saline solution with 0.1% TRITON X100). The variability was also measured for two reading (1 second each) 10 seconds apart. In the microplate design, the samples were positioned in next or far wells to test the overwhelming signal effect. We tested also the variability in case of the presence or absence of time gap between triplicates/dilution. Samples were prepared and analyzed as described below.

2. *In vitro* bioluminescence luciferase assays for Fluc and sGluc.

A. Fluc. The cells were lysed with 50 µl of 1x lysis buffer and incubated for 5 minutes in ice. 100µl of the Britelite solution (D.luciferine substrate + ATP + Co-A) was then added to 20µl supernatant of cell lysates using the automatic injectors of Orion II Microplate Luminometer. The measurements were taken over 10 seconds after 2.5 seconds delaying period. The positive control was the lysate of Fluc+ 4T1.2 cells, while the negative control was the lysis buffer (**Figure.7**).

B. sGluc. The tissue culture medium was filtered and centrifuged, then 50µl of Coelenterazine substrate (0.005 mg/ml, diluted in PBST) was added by the automatic injectors to only 2µl of the filtered media. The measurement was taken over 1 second after

2.5 seconds delaying period. The positive control was the conditioned media for HA++ 4T1.2 cells, while the negative control was the PBST.

***In vivo* assays.** All the *in vivo* assays have got the ethical committee approval with no conflict with the university of Queensland and Australian national guidelines. For the 4T1.2 orthotopic model, eight weeks old BALB/c mice (n=30) were implanted in the fourth mammary fat bad with 50µl of PBS containing $1x10^5$ HA++ cells (sGluc+Fluc+), or HA+ cells (sGluc+Fluc-), or parental cells (sGluc-Fluc-) as a negative control. The mammary tumors were palpable, but not measurable 5 days post injection. The primary tumor measurements were taken two times/week using an electronic caliper. Tumor volume were calculated using m1 × m1× m2 × 0.5236 (m1 signifies the little tumor axis and m2 the long axis) (**Figure.9A)**.

On specified days after 4T1.2 cells inoculation, tumor growth was monitored using *in vivo* bioluminescence imaging for Fluc upon intraperitoneally injection of D-luciferin (100 mg/kg). Imaging was accomplished using IVIS Spectrum - PerkinElmer CCD camera and subsequently analyzed with Living Image software (Caliper Life Sciences).

After six weeks, the primary tumors were surgically removed to allow metastasis growth. General anesthesia was induced by subcutaneous injection of a ketamine/xylazine mixture (80 mg/kg body weight ketamine and 10 mg/kg body weight xylazine) by intraperitoneal route (1 cc syringe). The mice were additionally anesthetized with oxygen containing 2.5% isofluorane.

The mice were sacrificed at different time points when the tumor size reached the limit of 1 cm2, or when showing any sign of distress such as difficulty in movement or rapid breathing.. All the sacrificed mice were subjected to careful post mortem examination, X-ray, and *ex*

vivo imaging for different organs. Moreover, lungs and bones (vertebral column, and pelvic limbs) were collected in either liquid nitrogen, or in PFA for subsequent analysis to localize and quantify the metastatic burden. The qPCR for mCherry genome sequence will be used for quantification, while the histological examination of formalin fixed samples will be used for localization (**Figure.8**).

***Ex vivo* sGluc blood assay.** 50 µl of blood were collected every three days from the tail vein in Na-Heparinized capillary tubes (Gelinlab). After centrifugation (4000 RPM/10 minutes), 2µl of the mouse plasma were tested as described above using the same protocol described for the sGluc *in vitro* bioluminescence luciferase assay.

Isolation, labelling, and flow cytometry analysis of adoptively transferred monocytes. The monocytes were isolated from bone marrow, spleen and cardiac blood from wild type (WT) and tumor bearing BALB/c mice under aseptic conditions.

Cells Isolation. Almost 1ml of blood/mouse was withdrawn from the heart of anesthetized mice using EDTA as anti-coagulant (100µl of 0.5M for 1 ml of blood). After culling the mice, the spleen and bone marrow cells were also collected. The Bone marrow cells were flushed out from femur and tibia of both hind limbs. After taking the spleen weight measurements using aseptic technique, the spleen was smashed with a 1 ml syringe through a sterile 40um cell strainer into a 50 ml conical tube. After washing the strainer with 10 ml MACS buffer (PBS, 0.5% BSA, 2 mM EDTA, pH 7.2) and centrifuging (1300 rpm/6min at 4ºC), the supernatant was discarded to make the splenocytes ready for RBCs lysis.

RBCs Lysis. In blood and splenocytes, red blood cell (RBCs) were then lysed using ACK lysis buffer (Gibco, cat. no. A1049201). 1ml of ACK buffer was added for each 100µl of

blood for 5 minutes. While for the spleen, 5-10 ml of ACK buffer was added according to spleen size and incubated on ice for 5 minutes. Blood and splenocytes were then centrifuged (1300 rpm/6min at 4ºC) and resuspension in MACS buffer. The hypotonic shock (hypotonic water lysis) was used for the RBCs lysis in bone marrow cells, where 1ml of Distilled Water (Gibco, cat. no. 15230-147) was added to cells just immediately before adding MACS buffer up to 50 ml to quench the lysis process. Bone marrow was then centrifuged (1300 rpm/6minute at 4ºC) and resuspended in MACS buffer.

FACS analysis of monocytes. Cell suspensions were incubated with anti-mouse FcγIII/II receptor (Cd16/Cd32) blocking antibodies for 15 min at 4°C and then stained with an antibody cocktail which included: the Anti-Mouse CD115 (c-fms)-APC, and Anti-Mouse Ly-6G (Gr-1) PerCP-Cyanine 5.5. To exclude dead cells from the analysis, cells were washed and resuspended in PBS containing 10 ng/ml 7-aminoactinomycin D (7-AAD). We purchased all flow cytometry antibodies (mouse specific) and reagents from e-Bioscience (San Diego, CA) unless else stated. 1/100 antibodies dilution with staining buffer was based on ideal results that we got from titration curves accomplished earlier to the study (data not shown). For FACS acquisition details see below.

Negative selection with MACS. For monocytes negative selection, we depleted the Ly6G+ cells by Magnetic Activated Cell Sorting (MACS). First, the cells were blocked with anti-mouse FcγIII/II receptor (Cd16/Cd32) blocking antibodies for 15 min at 4°C and then stained for 20 min at 4 °C with PerCP-Cy™5.5 Rat Anti-Mouse Ly-6G (BD Pharmingen™, cat. no. 560602, clone 1A8). Then, the Anti-Rat IgG MicroBeads (Miltenyi Biotec, cat. no. 130-048-501) were added for magnetically labelling the cells for 15 minutes at 4ºC. Subsequently, the suspension was loaded onto the magnetic field of autoMACS® Pro Separator (Miltenyi Biotec). The Ly6G– cells containing the monocytes were collected at the flow through (FT).

The total blood leukocyte numbers were determined by automated blood analyzer (Beckman Coulter Ac·T 10) with mouse setting.

Sorting the CD115+ Ly6G– cells. The FT (Ly6G–) were then centrifuged before labelling the cells with APC anti-mouse CD115 and APC/Cy7 anti-mouseCD11b monoclonal antibodies for sorting the monocytes out by fluorescence-activated cell sorting (FACS) by MoFlo® Astrios™ sorter (Beckman Coulter, Inc).

Investigating the Ly6G– CD115+ splenic monocytes homing ability after adoptive transfer of cells labelled with Cell Proliferation Dye eFluor® 450.

Dye preparation. Cell Proliferation eFluor® 450 (eBioscience) fluorescent dye was reconstituted in anhydrous DMSO as 10 mM stock solutions (stored with dessicant at − 20 °C).

Monocytes labelling. A final concentration of 20 μM of the dye was added to 5x10^6 splenic monocytes after resuspending in prewarmed PBS. This was followed by direct vortexing to the mixture to confirm fast consistent labelling of monocytes. Cells were incubated at 37 °C for 10 minutes in dark, then 4-5 volumes of cold RPMI 1640 supplemented with 10% FCS was added to wash the monocytes three times to minimize the cell toxicity. The labelled monocytes (5x10^6 cells) were then i.v injected into one of HA++ mouse which was subsequently killed after 5 days together with one control parental mouse to explore the recruiting of the labelled monocytes to primary tumor tissue and spleen, using flow cytometer analysis.

Flow cytometry of adoptively transferred monocytes.

1. Spleen. The spleen was first smashed and the resulting cell suspension was passed through 40 μm nylon filter and washed in cold phosphate buffered saline (PBS) containing 2mM EDTA and 0.5% Bovine Serum Albumin (BSA).

2. Tumor. The tumor was excised, smashed and digested by adding collagenase IV (0.2 mg/ml, Worthington), dispase (2 mg/ml, Gibco) and DNaseI (0.1 mg/ml, Roche) in PBS containing 2% fetal calf serum (FCS) for 20-30 min (according to tumor dimension) at 37°C in a shaking bath. The obtained cell suspension was first passed through a 40 μm filter and then washed in cold phosphate buffered saline (PBS) containing 2mM EDTA and 0.5% bovine serum albumin (BSA).

Cell suspensions were then incubated with anti-mouse FcγIII/II receptor (Cd16/Cd32) blocking antibodies for 15 min at 4°C and then stained for 30 minutes on ice with an antibody cocktail which included: the PerCP/Cy5.5 anti-mouse CD45, APC anti-mouse CD11b, and FITC anti-mouse F4/80.

FACS data acquisition and analysis. A BD LSR II flow cytometer (Becton Dickinson) and FlowJo software were used for acquisition and data analysis. The Biexponential transformations were corrected manually when needed. Fluorescence minus one (FMO) were used for gating analyses to discriminate negative and positive staining cell subpopulations, while the BD Comp Beads (BD Biosciences) single color stained samples were used as controls for compensation.

Statistical Analysis. The standard error of the mean (SEM) or mean ± standard deviation (SD) values were expressed as indicated.

IV. Results

Aim1: Generation and validation of a new tumor cell line expressing a secreted form of Luciferase (4T1.2sLuc).

Generation of 4T1.2sLuc by lentivirus transduction. Lentiviral based gene-transfer technology was used to generate new 4T1.2 cell lines (4T1.2sLuc) that able to produce a secreted form of luciferase. Cells were transduced, selected and then validated *in vitro* and *in vivo* according to the scheme reported in **Figure.3**.

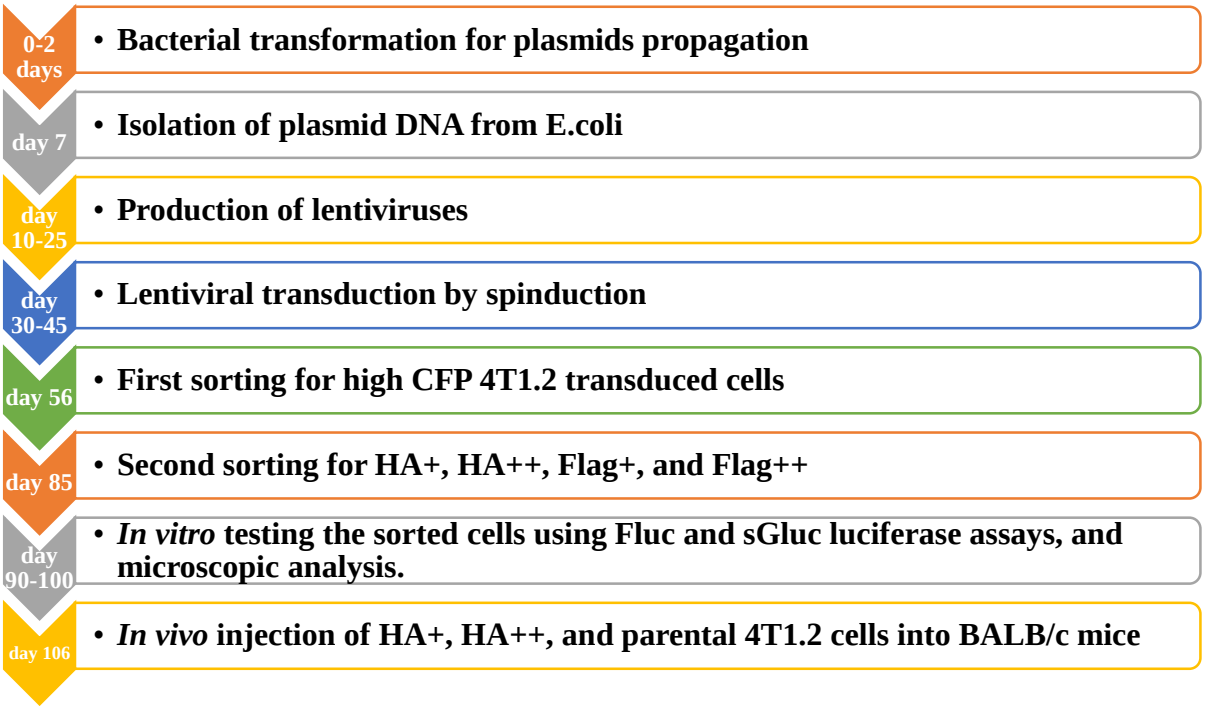

Figure.3: Schematic representation of the experimental design

We used two lentiviral vectors (sGlucFlag, and sGlucHA, **Figure.4A**) consisting of the sGluc cDNA fused at its C-terminus to either one of two epitope tags (Flag or HA), downstream to the ubiquitous cytomegalovirus (CMV) promoter. The two lentiviral vectors also express cerulean fluorescent protein (CFP) as an additional reporter gene, whose cDNA is separated from the sGluctag cDNA by an internal ribosomal entry site (IRES) element. We then

transduced these two vectors into murine 4T1.2 cells already stably expressing Fluc and the mCherry fluorescent reporter protein to generate two new cell lines, each stably expressing one of the two sGluc vectors together with the Fluc vector.

Sorting and Enrichment. To enrich for sGluc expressing cells, we performed Fluorescence-activated cell sorting (FACS). A first round of selection was performed 10 days after transduction by sorting CFP positive cells. However, as shown in **Figure.4B**, the purity of the sorted cells was relatively low (> 60% for both Flag and the Ha-4T1.2sLuc cells). Fluorescent microscopy analysis for mCherry and CFP confirmed that only a small proportion of cells were expressing both fluorescent proteins (**Figure.4C**).

One month later, a second round of selection was performed to isolate: single positive ($CFP^{+}mCherry^{neg}$) and double positive cells ($CFP^{+}mCherry^{+}$) for each tag (HA and Flag). We then sorted both the double and single positives 4T1.2 cells to be able to investigate the potential immunogenicity of secreted and/or intracellular luciferase protein that could lead to a severe decline of tumor growth and progression in immunocompetent mice (70). As shown in **Figure.4D**, HA cells had a higher purity profile after sorting then Flag cells: 84% and 82% for the two HA cell lines versus 78% and 80% for the Flag cell lines.

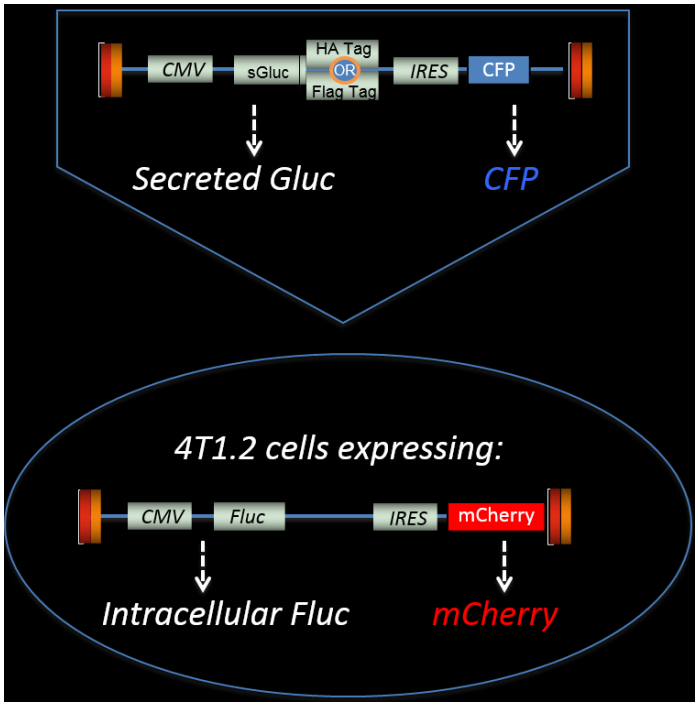

A. Lentiviral transduction of 4T1.2 cells

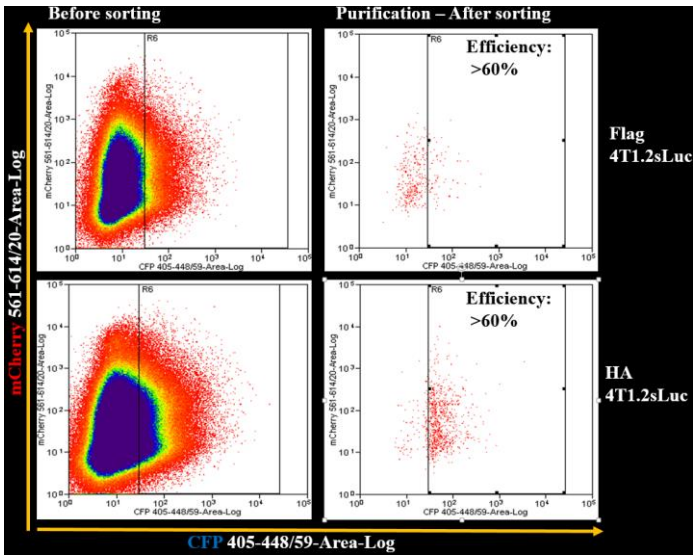

B. First round of sorting for transduced 4T1.2 cells

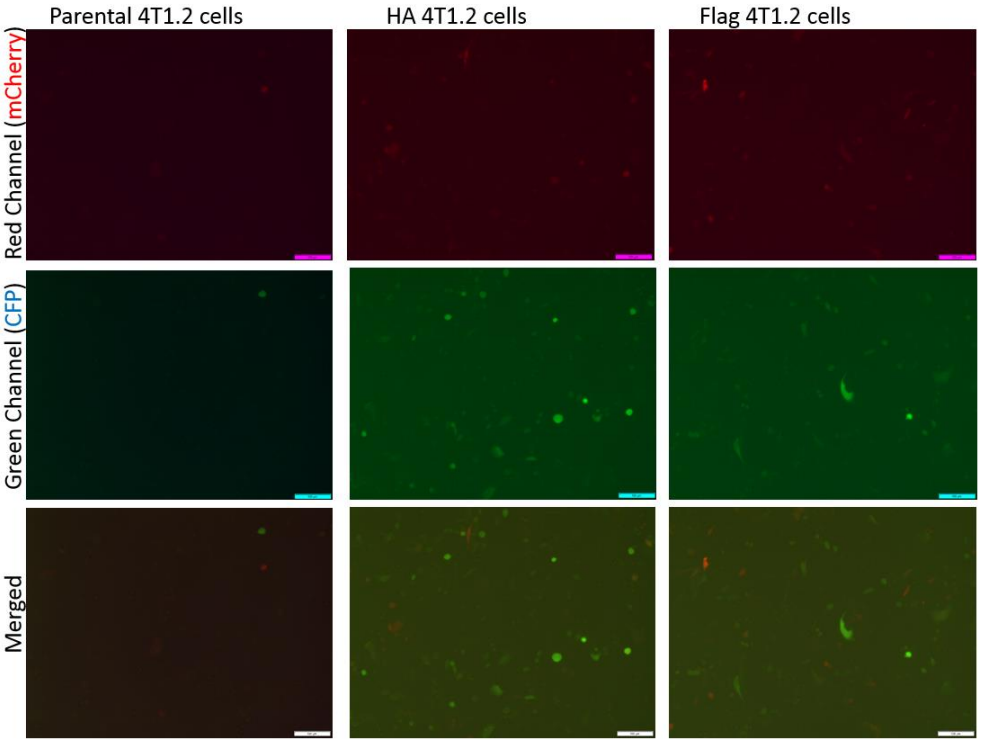

C. CFP and mCherry under fluorescence microscope

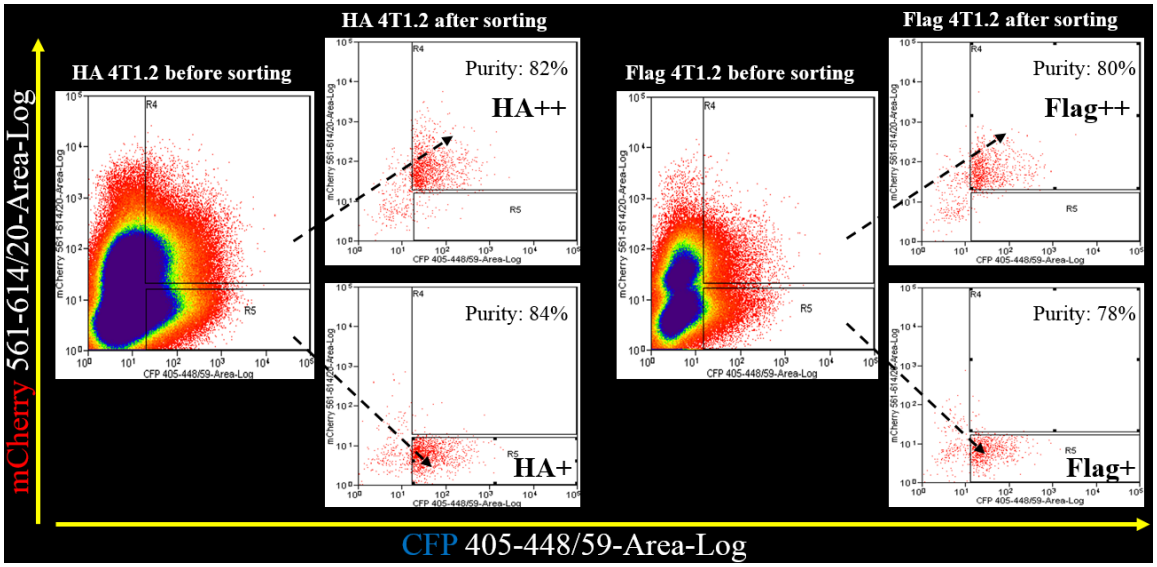

D. Second round of sorting for transduced 4T1.2 cells

Figure.4 Lentiviral transduction of 4T1.2 cells and sorting. A. A lentiviral vector was used to insert the transgene encoding for the secreted Gaussia luciferase with its CFP reporter into the 4T1.2 mammary tumor cell line, which were already transduced with the intracellular Firefly luciferase and its mCherry reporter. **B**. Transduced 4T1.2 cells were sorted by FACS

using the CFP reporter gene to select the highest sGluc producing cells, **C.** Fluorescence microscopy was used to check CFP and mCherry production. **D**. Second round of sorting by FACS using both CFP and mCherry reporter genes to isolate single positives (HA+, Flag+) and double positives (HA++, Flag++) cells.

Post sorting analysis. CFP and mCherry levels were re-evaluated 8 days after sorting by FACS analysis and compared with 4T1.2 cells that not transduced with any luciferase vector (parental cells). As shown in **Figure.5**, the levels of both fluorescent proteins were drastically reduced after culturing, indicating possible silencing of the entire viral construct or loss functionality of the IRES sequence resulting in silencing of the reporter genes only (see luciferase assay below for further discussion). Despite downregulation both CFP and mCherry reporter genes in HA+ and Flag+ cells, there were no double positive CFP+mCherry+ cells. Instead, a large proportion of cells were double negative in all sorted cells lines. We decided to only use HA+, HA++ cells for further analysis because they showed a higher growth rate *in vitro* (data not shown).

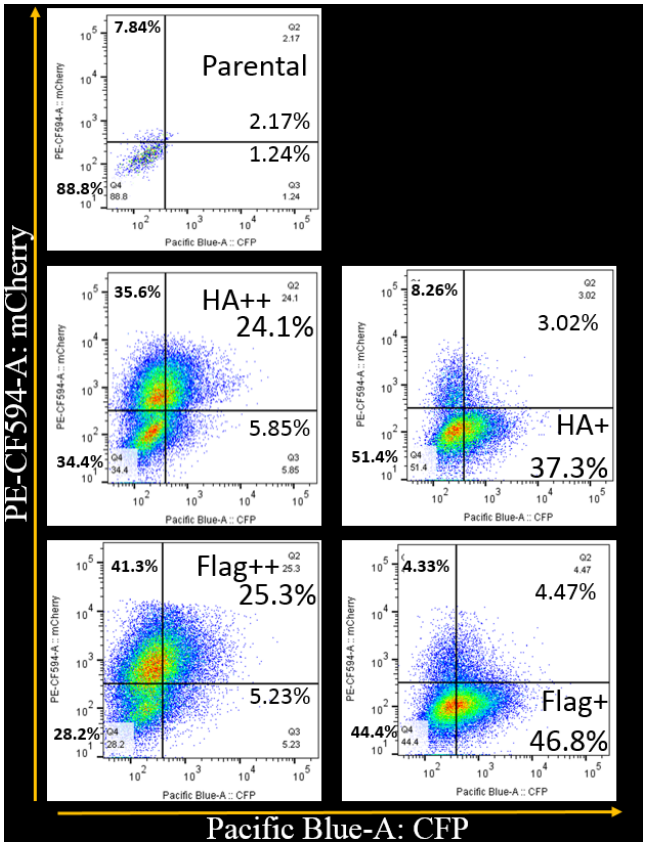

Figure.5: Post sorting flow cytometric analysis. This analysis shows the comparative levels of CFP (sGluc reporter) and mCherry (Fluc reporter) in the five 4T1.2 cell lines (parental, HA+, HA++, Flag+, and Flag++). The cells were maintained in standard tissue culture conditions as described in Materials and Methods. Debris (SSC-A vs. FSC-A) and doublets (FSC-H vs. FSC-A) were excluded. Frequencies of cells in each sub-gate (after doublet and debris elimination) are stated as a fraction of live cells.

Setting up the *in vitro* luciferase assays. The Orion II Microplate Luminometer was set up to measure the bioluminescent signal produced by sGluc and Fluc upon addition of their specific substrates (coelenterazine and britelite respectively). Preliminary experiments were performed to test sensitivity and linearity.

1. Fluc. 4T1.2 cells expressing Fluc only and parental 4T1.2 cells that do not express any luciferase, were used to prepare total cell extracts. Increasing amounts of total proteins from Fluc 4T1.2 cells (from 0 µg to 103 µg) were mixed with decreasing amount of total proteins from parental 4T1.2 cells. The bioluminescent signals were directly proportional to the amount of total proteins from Fluc 4T1.2 cells. The signals were measured instantly and 12 seconds after adding the substrate. As expected, the signal intensity slightly dropped over time and according to the R^2 value of each interpolated line, we decided to use the first measurement (**Figure.6**-left panel).

2. Gluc. To measure the bioluminescence derived from sGluc protein secreted by transduced HA++ 4T1.2 cells, 500000 cells were plated and conditioned medium was collected after 24h in culture. Serial 1:10 dilutions were used to test sensitivity and linearity in the bioluminescent signal. Despite high variability within triplicates, we obtained a good R^2 value for the interpolated curve (R^2 = 0.9995, **Figure.6**-right panel). The instrument was sensitive until 1/1000 dilution, which is equal to 500 cells. 50µl of substrate was the optimal concentration to use for the analysis and empty wells gave signals that range between 1000-2500 RLU, which led us to consider any signal within this range as negative.

Testing the samples in near or far wells did not change the results, indicating that there was no interference between adjacent wells (data not shown). Similarly, introduction of time gaps between the triplicate measurements did not change the outcomes (data not shown).

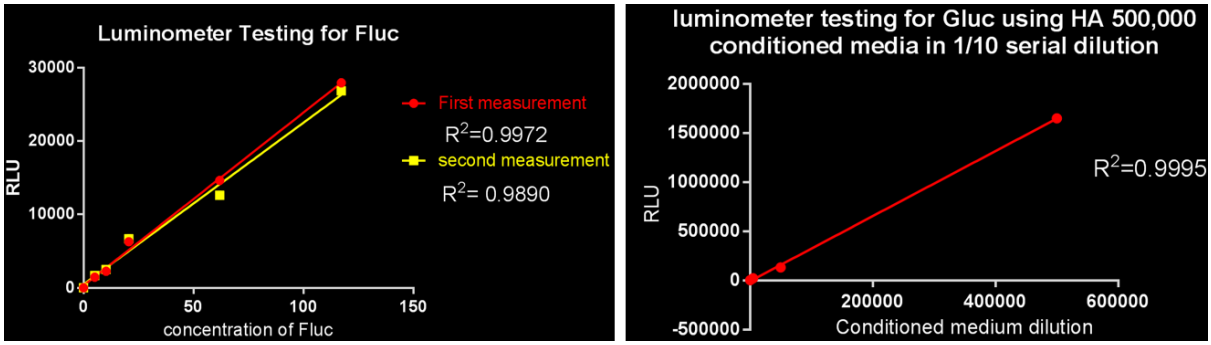

Figure.6 Setting up *in vitro* bioluminescence assays using the Orion II Microplate Luminometer. The Fluc signals (right) were measured in decreasing amount of total cell extracts at two time points after substrate addition, as described in materials and methods. For sGluc assay (left), the measurements were taken using serial 1:10 dilutions of HA++ 4T1.2 conditioned medium. This graphs were plotted by GraphPad Prism software 6.0 (San Diego, CA, USA), and the regression coefficient (R^2) were calculated for each curve.

***In vitro* validation of luciferase production in transduced 4T1.2 cells.** Single positive cells (HA+) were expected to express sGluc only and double positive cells (HA++) were expected to express both luciferases, while the Parental 4T1.2 cells were used as negative control. Twenty four hours after plating different concentrations of cells, total cell lysates and conditioned media were collected and tested for the levels of Fluc and sGluc respectively. As shown in **Figure.7**, parental cells were negative for both sGluc and Fluc. As expected, the sGluc levels were directly proportional to the number of both HA+, and HA++ cells plated (**Figure.7**-left panel). However, unexpectedly, both cell lines were also positive for Fluc with a high signal directly proportional to the number of cells plated (**Figure.7**-right panel). These data are not in agreement with the reporter gene profile after sorting. However, strong silencing of IRES-mCherry but not Fluc in culture might explain the observed results (see FACs analysis post sorting, **Figure.5**).

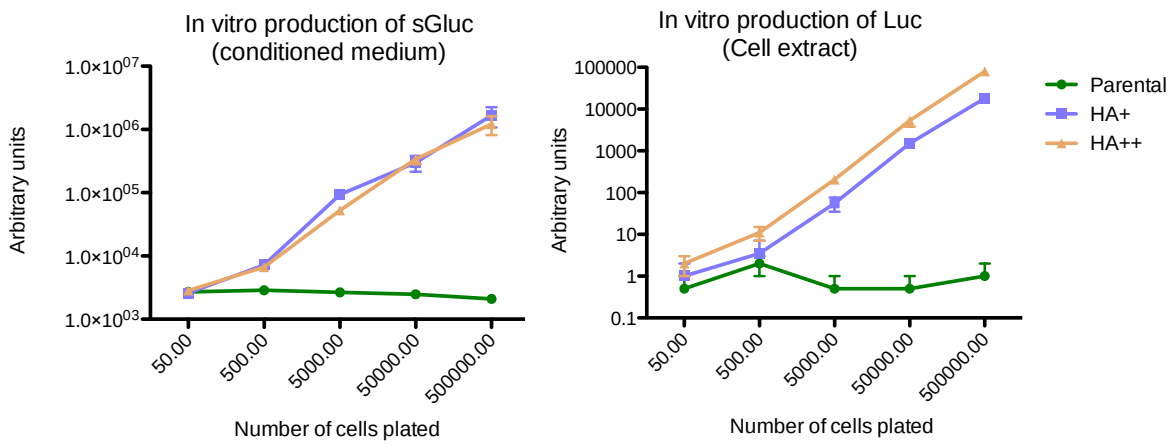

Figure.7: *In vitro* bioluminescence assays. sGluc (left) and Fluc (right) activity in 4T1.2 cells (HA+, HA++, parental) expressing different levels with respect to cell number and cell proliferation over 24 hours. The measurement values are given in arbitrary units (a.u.). Error bars represent SEM; n = 3 measurements.

Characterization of the *in vivo* growth and dissemination of 4T1.2sLuc cells. 4T1.2 tumor cells were orthotopically injected into the fourth inguinal mammary gland of immunocompetent Balb/c mice. Ten mice were injected with each of the following cell lines: HA+, HA++, and parental. Tumor growth, *ex vivo* bioluminescence from sGluc, *in vivo* bioluminescence from Fluc, and x-rays were measured as described in **Figure.8**.

0 – 2nd week	2nd – 5th week	6th week
• Orthotopic injection of tumor cells (Parental, HA+, or HA++) • 10mice/cell line	• Tumor size measurement (2times/week). • sGluc Measurement in blood ex vivo (2times/week). • Fluc and mCherry analysis in vivo by IVIS (1time/week). • X-ray was used for bone metastasis detection (1time/week).	• The Primary tumor was removed • The tumor metastasis was followed using sGluc, Fluc, and X-ray measurements. • Distressed mice were sacrified, and subjected to ex vivo examination of isolated organs. • Organs were collected for Histology and qPCR.

Figure.8: Schematic representation of the *in vivo* experimental design.

1. Tumor growth. After transplantation of the 4T1.2 tumor cells in the fourth inguinal mammary glands of thirty mice. 10 mice were injected for each cell line (HA+, HA++, parental). All the mice except 9 mice developed primary tumors which kept growing steadily to reach the maximum limit of 1cm^2 after almost 6 weeks. The growth did not show dissimilarity between the three groups of mice (**Figure.9A**). Seven out of eight mice that did not develop primary tumors were euthanized after 2-3 weeks because severe signs of distress and weakness (see below for sGluc and Fluc analysis in these mice). Upon sacrifice and autopsy these mice were shown to have intraperitoneal tumor tissues that complicated with the internal abdominal organs.

2. Extracellular secreted Gaussia luciferase (sGluc) measurements. As the tumor were growing, we determined the levels of sGluc activity released into the blood of tumor bearing mice over time. Blood serum of each mouse was analysed as described in material and methods. Serum from mice injected with parental 4T1.2 cells was used as negative control. Conditioned medium from HA++ cells was included as positive control for sGluc activity. As

reported in **Table.1**, 50-60% of the injected mice showed sGluc in their blood 5 days after orthotopical injection of tumor cells. Surprisingly, all the mice that were not showing orthotopic growth of HA+ and HA++ tumor cells (improperly injected mice) showed a positive and high signals. However, 12 days after tumor cell injection, the sGluc signal dropped down to the same level as the mice injected with parental 4T1.2 cells (**Figure.9B**).

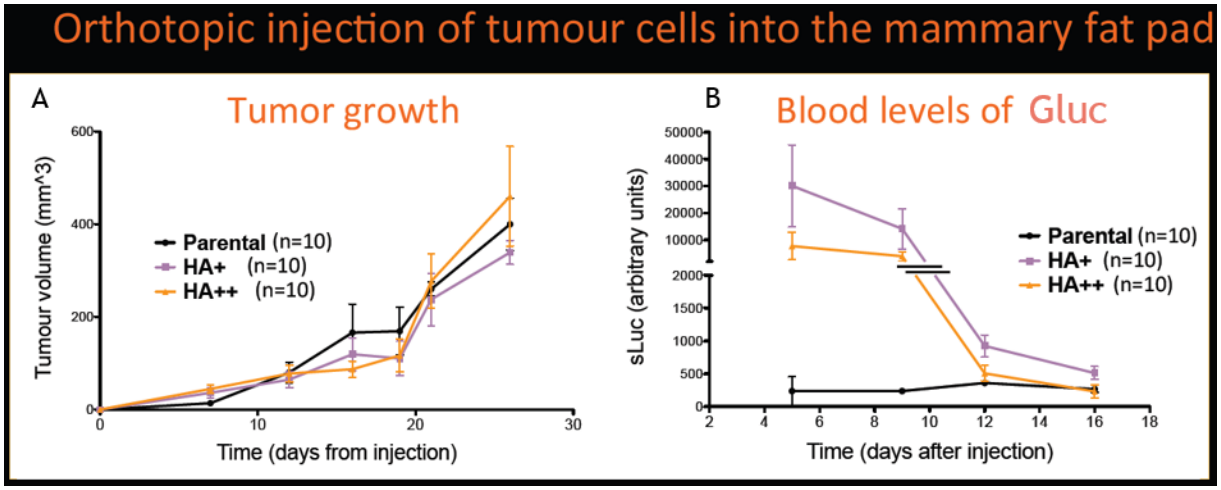

Figure.9: Measurements of tumor volumes and sGluc. **A.** Tumor volumes were taken twice a week and calculated using m1 × m1× m2 × 0.5236 (m1 refers to the shorter tumor axis while m2 represents the longer axis). **B.** sGluc bioluminescent signals in the blood of tumor bearing mice over the first two weeks after tumor cells injection. Error bars represent SEM; n = 3 measurements.

Tumor cells injected	Improperly injected mice*	sGluc Signal				
		D5			D9	D12
		All mice	Improperly injected	Properly injected	All mice	All mice
Parental	3/10 (30%)	0/10 (0%)	0/3 (0%)	0/7 (0%)	0/10 (0%)	0/10 (0%)
HA+	3/10 (30%)	6/10 (60%)	3/3 (100%)	3/7 (43%)	7/10 (70%)	0/10 (0%)
HA++	1/10 (10%)	5/10 (50%)	1/1 (100%)	4/9 (44%)	4/10 (40%)	0/10 (0%)

Table.1: Number and % of sGluc+ mice. sGluc measurements show the gradual decrease in sGluc+ mice, and the difference between properly and improperly (*) injected mice.

(*) Improperly injected mice were characterized by swollen abdomen, tumor development in the abdominal cavity, and no primary tumor growth in the mammary glands. Post tumor cells injections, those mice also showed strong sGluc signals in the first week, early strong positive Fluc signals by IVIS, and died within the first 2 weeks.

3. Intracellular Firefly luciferase (Fluc) measurements. We monitored primary and metastatic tumor growth *in vivo* by Fluc bioluminescence imaging. In 80% of the Fluc+ mice, the signal detected in the primary tumor was directly correlated with the primary tumor growth as shown for HA++ injected mice #82 and #83 in **Figure.10A**. However, this signal was not always associated with the mCherry florescence signal (**Figure.10B),** which highlighting the poor correlation between Fluc and its reporter gene expression.

To identify the anatomical localization of the *in vivo* bioluminescent signal, mice were sacrificed and organs were re-analysed *ex vivo* directly after the *in vivo* imaging. Unexpectedly, the signal observed *in vivo* was often lost *ex vivo* (**Figure.10C)**. Moreover there was no Fluc signal *in vivo* and *ex vivo* in the lungs of 84% of the HA+ and HA++ mice that had lung metastasis (**Figure.10C** and **Table.2**).

One of the noticeable observations is that some mice had positive signals at early time points in the location of primary tumor, but then that signal was lost despite the primary tumor growth and presence of metastasis in the lung (**Figure.10C)**. Another important observation is that the primary tumor is not homogenously emitting bioluminescent signal *ex vivo* imaging, which might indicate the presence of different cell populations within the tumor mass (**Figure.10D)**.

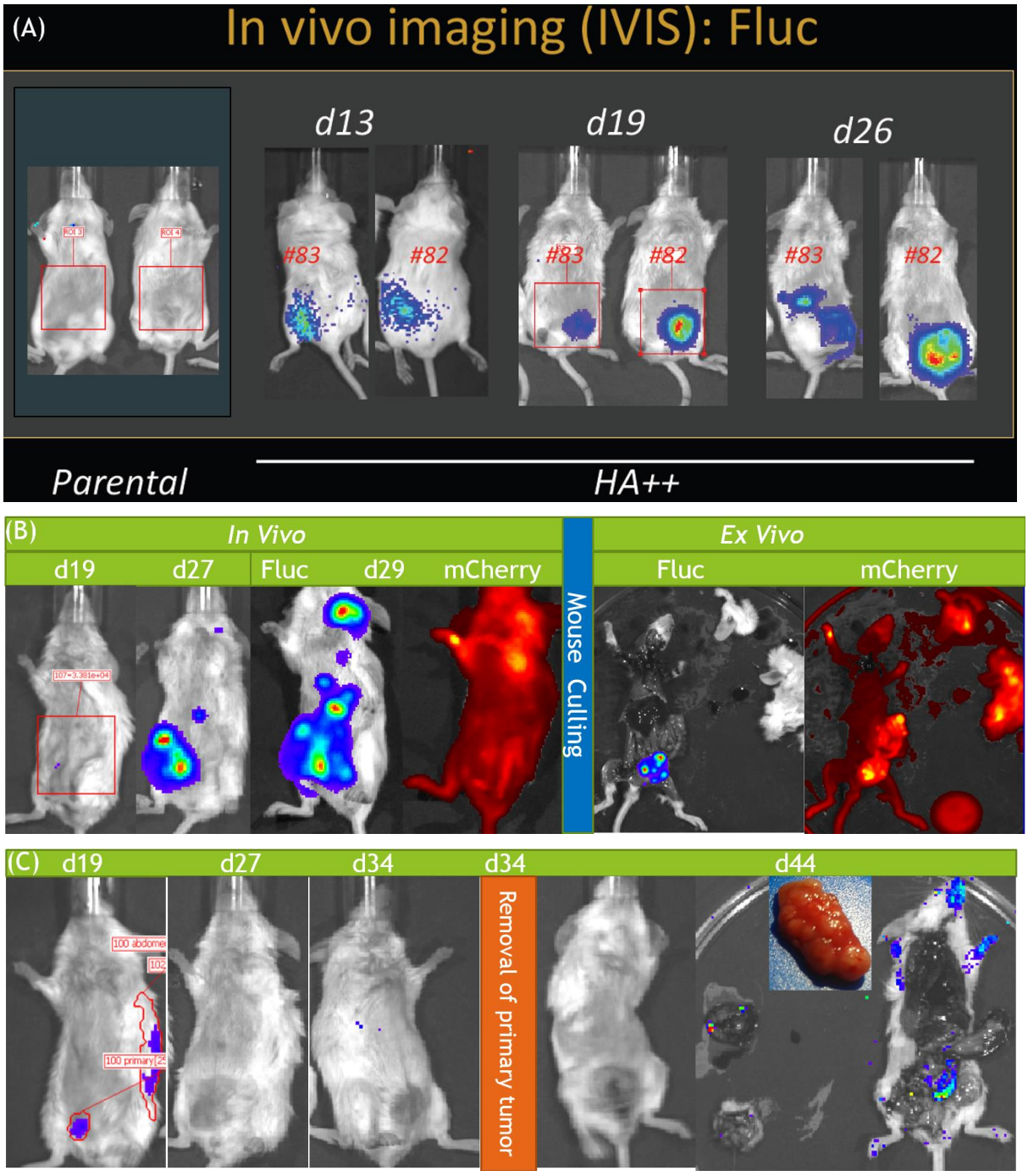

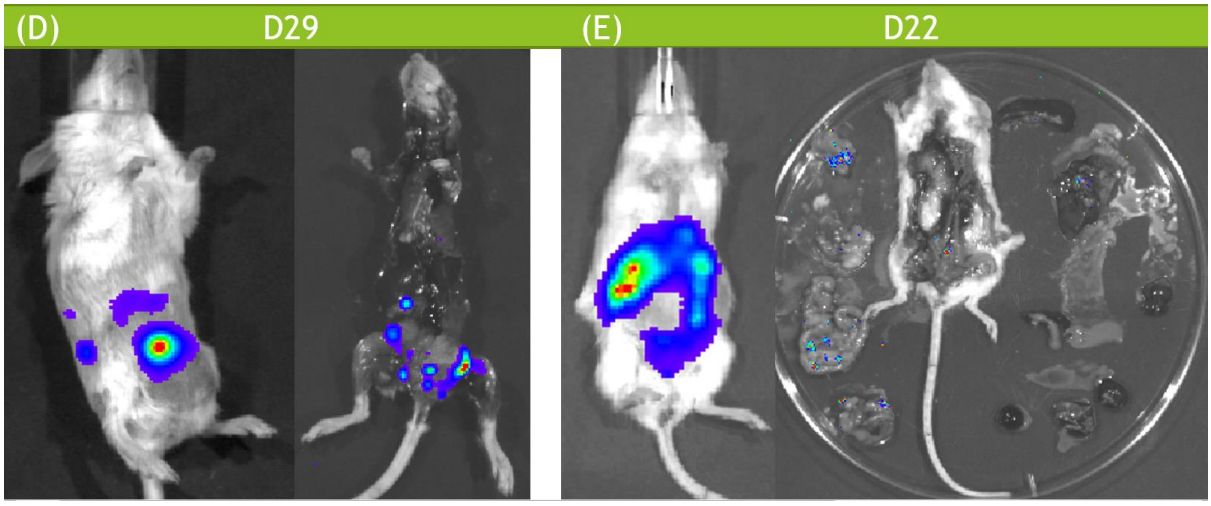

Figure.10: Bioluminescence and fluorescence imaging of representative mice using IVIS. *In vivo* bioluminescence analysis for localization and quantification of primary and metastatic tumors was performed twice a week by intraperitoneal injection of D-luciferin substrate. **(A)** Fluc bioluminescence imaging of two representative HA++ mice (#82, and #83) and two parental mice. Primary tumor growth correlated with a gradual increase in the bioluminescent signal over time in contrast to the negative parental mice **(B)** Comparison between mCherry and Fluc signals showing inconsistent overlap in a representative HA++ mouse. **(C)** Representative HA+ mouse showing disappearance of the bioluminescent signal, but not of the tumor mass at day 27 upon tumor cells injection. The mouse was sacrificed after day 44 and several lung metastasis were observed that had no Fluc signal. **(D)** Representative HA++ mouse showing that the bioluminescent signal can be observed in a limited parts of the tumor mass. **(E)** Representative HA++ mouse (one of the improperly injected mice) showing that the peritoneal signal is easily lost after just 5 minutes from euthanasia.

4. X-ray. In order to check the presence of bone metastasis *in vivo*, we used Faxitron cabinet for X-ray imaging to monitor the mice skeletal system regularly. More than 60% of the animals showed improper gait or hunching posture after 26 days of tumor cells injections. However, we could not record any positive signals by IVIS for Fluc in the bones. By x-ray analysis clear osteolytic metastasis in the bones were very rarely seen (**Figure.11**).

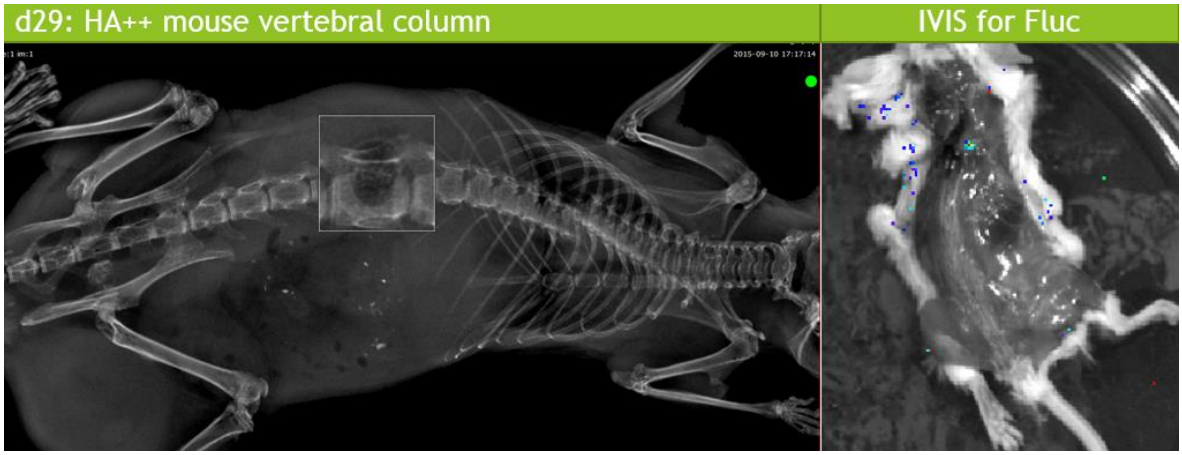

Figure.11: Digital X-ray image of a HA++ representative mouse. Xray (Left) shows a large tumor in the body of the first lumbar vertebral bone with obvious sclerotic rim, and protuberant bone expansion but no cortical destruction. The *ex vivo* bioluminescence imaging (right) of Fluc for the same mouse by IVIS (three minutes after euthanizing the mouse) did not show any signals.

5. Primary tumor removal and subsequent measurements. In a subset of animals the primary tumors were removed by laparotomy six weeks after tumor injection. Soon after the mice were culled because the signs of distress, plus lungs and bones were dissected for histological examinations and qPCR of mCherry protein.

		D19		D27		Surgery	At sacrifice					
		in vivo Fluc		*in vivo* Fluc			*in vivo* Fluc		*ex vivo* Fluc		Autopsy	
	ID	Primary	Metastasis	Primary	Metastasis		Primary	Metastasis	Primary	Metastasis	Primary	Metastasis
Parental	84	✗	✗	✗	✗	NA	✗	✗	✗	✗	✓	✗
	85	✗	✗	✗	✗	NA	✗	✗	✗	✗	✓	✗
	86	✗	✗	NA	NA	NA	NA	NA	NA	NA	✗	✓
	87	✗	✗	✗	✗	✗✗✗	✗	✗	✗	✗	✓	✓
	88	✗	✗	NA	NA	NA	NA	NA	NA	NA	✗	✓
	89	✗	✗	NA	NA	NA	NA	NA	NA	NA	✓	✗
	90	✗	✗	✗	✗	NA	NA	NA	NA	NA	✓	✗
	91	✗	✗	✗	✗	NA	✗	✗	✗	✗	✓	✗
	92	✗	✗	✗	✗	NA	✗	✗	✗	✗	✓	✗
	93	✗	✗	✗	✗	✗✗✗	✗	✗	✗	✗	✓	ϕ
Stat		**0%**	**0%**	**0%**	**0%**	**20%**	**0%**	**0%**	**0%**	**0%**	**80%**	**40%**
HA+	94	✓	✗	NA	NA	NA	NA	NA	NA	NA	NA	NA
	95	✓	✗	✓	✗	✗✗✗	✓	✓	✓	✗	✓	ϕ
	96	✓	✗	✓	✗	✗✗✗	✓	✓	✓	✗	✓	✓
	97	NA	NA	NA	NA	NA	NA	NA	NA	NA	✗	✓
	98	✓	✗	NA	NA	NA	NA	NA	NA	NA	✗	✓
	99	✓	✗	✓	✗	✗✗✗	✗	✗	✗	✗	✓	ϕ
	100	✓	✓	✗	✗	✗✗✗	✗	✗	✗	✗	✓	ϕ
	101	✓	✗	✗	✗	✗✗✗	✗	ϕ	✗	ϕ	✓	ϕ✓
	102	✓	✓	NA	NA	NA	NA	NA	NA	NA	✗	✓
	103	✓	✗	✓	✗	NA	✓	✓	NA	NA	✗	✗
Stat		**90%**	**20%**	**40%**	**0%**	**50%**	**30%**	**40%**	**20%**	**10%**	**50%**	**90%**

HA++	79	✗	✗	✗	✗	NA	✗	✗	✗	✗	✗	✗
	80	✓	✗	✓	✗	✕✕✕	✗	✗	✗	✗	✓	✗
	81	✓	✗	✓	✗	NA	NA	NA	NA	NA	✓	✗
	82	✓	✗	✓	✓	✕✕✕	✓	✗	✓	✗	✓	✗
	83	✓	✗	✓	✗	✕✕✕	✓	✓	✓	✓	✓	✓
	104	✓	✗	✗	✗	✕✕✕	✓	✗	✓	✗	✓	Ω
	105	✓	✓	NA	NA	NA	✓	✓	✗	✗	✗	✓
	106	✗	✗	✗	✗	✕✕✕	✗	✗	✓	✗	✓	ϕ✓
	107	✗	✗	✓	✗	✕✕✕	✓	✓	✓	✗	✓	✓
	108	✓	✗	✓	✗	✕✕✕	✓	✓	✗	✗	✓	ϕ
Stat		**70%**	**10%**	**60%**	**10%**	**70%**	**60%**	**40%**	**50%**	**10%**	**80%**	**60%**

Table.2: Lists of the *in vivo* assay observations to compare the primary and metastatic tumor growth. The tumor growth was measured by caliper, Fluc imaging in two representative time points (Day 19th, and 27th) before primary tumor removal, and at different time points before sacrificing (*in vivo* and *ex vivo*). The table also summarizes the post mortem examination observed by eye for the sacrificed mice. Sometimes we could not analyse the mice because of time limitation or animal death. Colours and symbols are as explained in the legend below.

✓	Yes
ϕ	Lung metastasis
Ω	bone metastasis
ϕ✓	Abdominal and lung metastasis
✗	No
NA	Not analysed
✕✕✕	Primary tum removal

Aim2: Adoptive transfer of mature monocytes into tumor bearing mice for testing their homing ability.

We are considering adoptive transfer of mature monocytes as an alternative to autologous HSCs transplantation for the delivery of IFNα by TEMs. To develop this approach we needed to set up four steps. Step 1 is to identify the best source of monocyte in our experimental mouse model. Step 2 is to design an efficient purification protocol. Step 3 is to optimize an *ex vivo* labeling protocol. Step 4 is to test the monocytes homing ability *in vivo* upon injection into tumor bearing mice.

Isolation and sorting. As first we tested the bone marrow from a wild type mouse as possible source of mature monocytes which were identified as CD115+ cells. We also investigated whether lysis of red blood cells (RBCs) had any possible negative effects on our final desired CD115+ monocytes. Toward this purpose, bone marrow cells from one representative mouse was analyzed by FACS before and after RBCs lysis for the percentage of CD115+ cells. The CD115+ live cells were found in a higher percentage after RBCs lysis (**Figure.12**). Therefore, we decided to sort for CD115+ cells from the RBCs lysed sample. As shown in **Figure.13**, CD115+ monocytes were efficiently isolated from total bone marrow with a purity of 92%. Moreover, all CD115+ cells were also CD11b+ which confirm their myeloid origin. However, despite the high purity after sorting, the absolute number of CD115+ cells that were recovered from the bone marrow was very low.

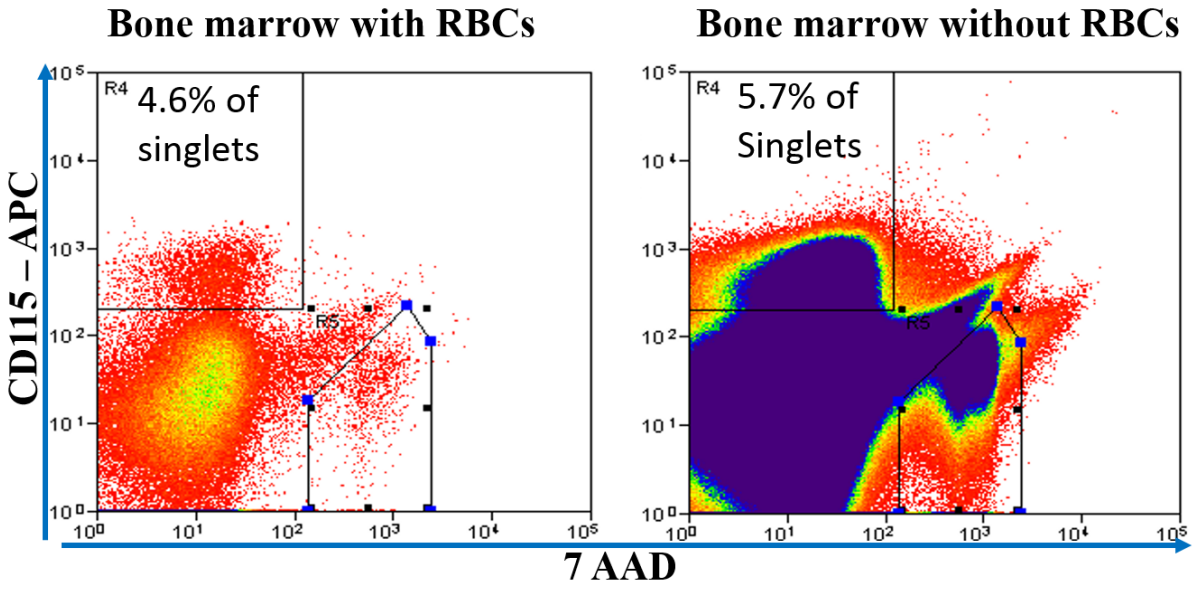

Figure.12 Representative flow cytometry analysis of bone marrow cells comparing the percentage of CD115+ cells before and after blood cell lysis. The percentages of CD115+ singlet cells in bone marrow after RBC lysis (Right) was greater than before RBC lysis (Left) with no change in the percentage of dead cells.

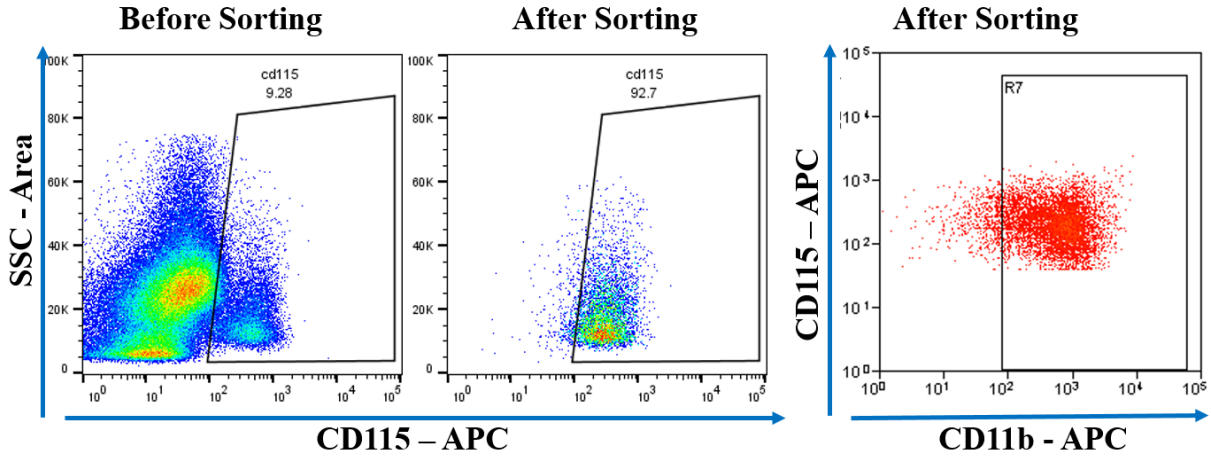

Figure.13 Immunophenotyping and sorting of CD115+ bone marrow cells. The sorted CD115+ cells were highly pure, but low in number (Left). The majority of the sorted cells were CD11b+ (right). Debris (SSC-A vs. FSC-A) and doublets (FSC-H vs. FSC-A) were excluded.

Because tumor-bearing mice are known to markedly expand their myeloid compartment in the bone marrow and peripheral blood, with a decrease in erythroid and lymphoid populations (71), we decided to investigate whether tumor bearing mice might represent a better source of monocytes. We, therefore, compared the percentage and absolute numbers of CD115+ monocytes in tumor bearing versus non-tumor bearing mice in different organs: bone marrow, blood and spleen (**Figure.14**). In addition to CD115+, 10^6 cells from each organ were also stained for the myeloid marker CD11b and the granulocytic marker Ly6G.

As shown in **Figure.14** and summarized in **Table.3**, tumor bearing mice had higher percentage of CD115+ monocytes in all organs analyzed. Moreover, spleen and blood of tumor bearing mice had the highest expected absolute numbers of monocytes. Finally, these data also indicate that most CD115+ cells are negative for Ly6G and that Ly6G+ cells represent the largest fraction of cells in the spleen and blood of tumor bearing mice.

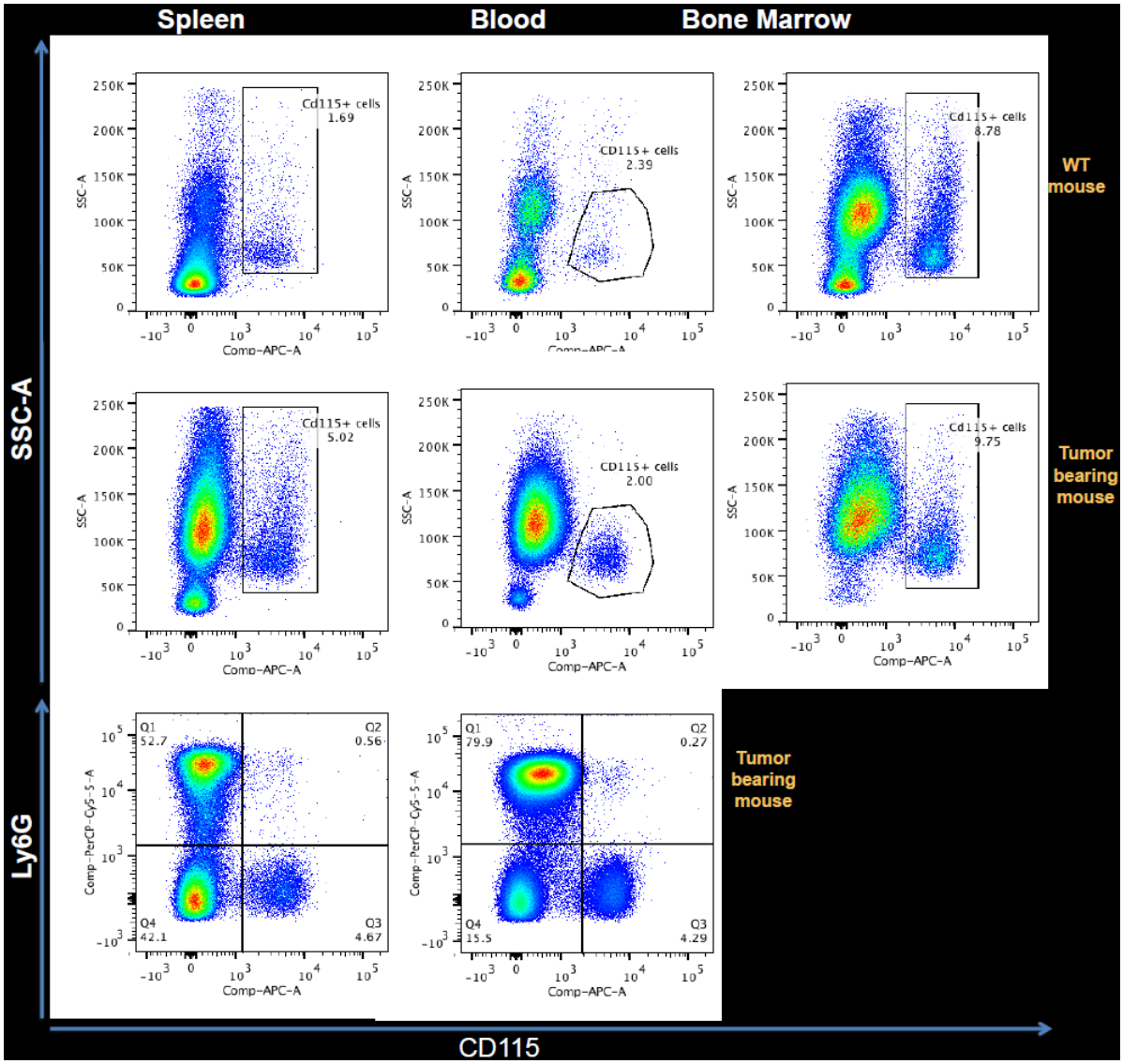

Figure.14: Total mouse splenocytes, WBCs, and bone marrow cells from non-bearing wildtype (wt) versus tumor bearing BALB/c mice. The cells were prepared as described in Materials and Methods and analyzed by FACS for the percentage of CD115+ cells. For the analysis, debris (SSC-A vs. FSC-A) and doublets (FSC-H vs. FSC-A) were excluded after gating on live cells. The percentage of CD115+ cells was calculated gating CD115+ cells against SSC (upper panel). Addition of Ly6G into the analysis was used to confirm that most CD115+ cells are Ly6G negative. The possible CD115+ cells that could be isolated based on this analysis were summarized in (**Table.3**).

	SPLEEN		BLOOD		Bone Marrow	
	wt	tum	wt	tum	wt	tum
Tot WBCs/ mouse (x10^6)	42.5	1656	NA	234.5	21.5	31
%CD115$^+$	1.7	5.02	2.4	2	8.8	9.7
Tot. monocytes (x10^6)	0.72	**83**	NA	**4.69**	1.89	3

Table.3: List of numbers and percentages of isolated white blood cells and the possible CD115+ sorted cells in spleen, blood, and bone marrow of both wild type (wt) and tumor bearing mice (tum). The numbers and percentages were calculated after applying the percentages that we got by flow cytometry (**Figure.14**) on the total leukocytic count calculated by the automated blood analyzer. The highest CD115+ cells were highlighted in blue color.

Based on the FACS data, we designed a purification protocol for the isolation of CD115+ monocytes from the spleen and blood of three tumor bearing mice. To reduce the time required for sorting, we first enriched the monocytes by negatively selecting Ly6G+ cells by Magnetic-activated cell sorting (MACS) (**Figure.15**). Anti-CD115 antibodies were then used to stain the monocytes in the flow through (FT) before the final cell sorting step.

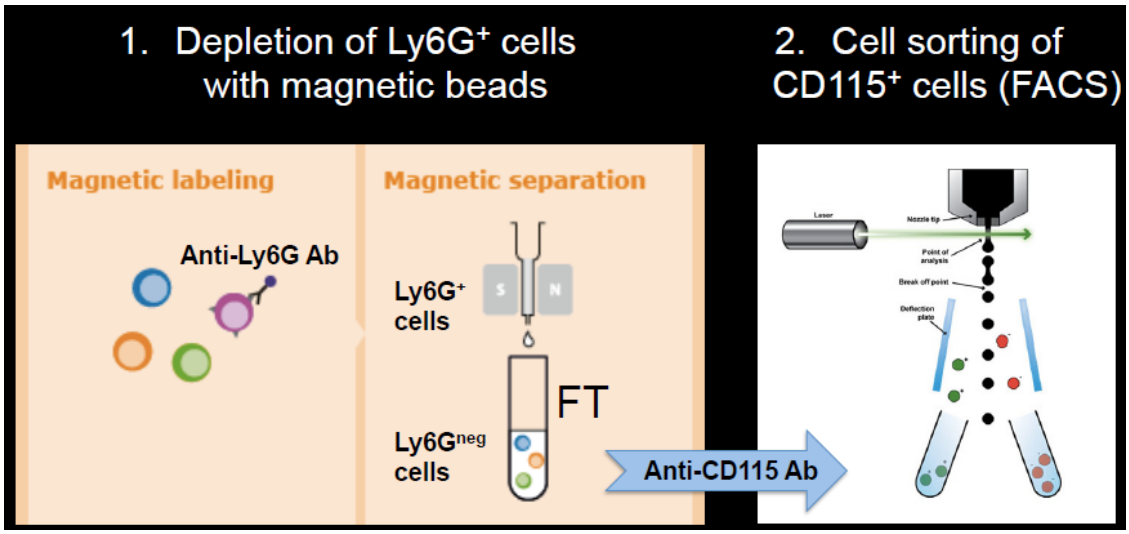

Figure.15: CD115+ Monocytes sorting strategy. The Ly6G+ cells were depleted from WBCs using Anti-Ly6G magnetic beads and the Auto-MACS system, before sorting CD115+ monocytes from the flow through (FT) by FACS. The photos adapted from ref. (72, 73) with modifications.

Unexpectedly, after negative selection with the AUTO-MACS, we did not observe any enrichment in CD115+ monocytes. On the contrary, the percentages and MFI of CD115+ cells was dramatically reduced in both spleen and blood, thus compromising the second step of isolation by FACS (data not shown). We still need to investigate whether this happens because of the monocytes activation, CD115 receptor internalization, or a technical problem in the MACS step. To overcome this problem and try to obtain some monocytes to inject, we stained the remaining spleens with CD115 and performed cell sorting as described in **Figure.13**. As before, the recovery was very low (5.05*10^6 CD115+ cells with 70% purification efficacy, which represent almost 3% of live cells) and the number of CD115+ cells recovered was sufficient to inject one recipient mouse only (data not shown - see below for adoptive transfer).

Because we were unsuccessful in enriching the monocytes properly using the strategy mentioned above, we are now investigating whether we could use a cocktail of antibodies to deplete all hematopoietic cells, but the $CD11b^{+}Ly6G^{neg}$ population, which according to our FACS data should be strongly enriched in CD115+ monocytes (**Figure.16**).

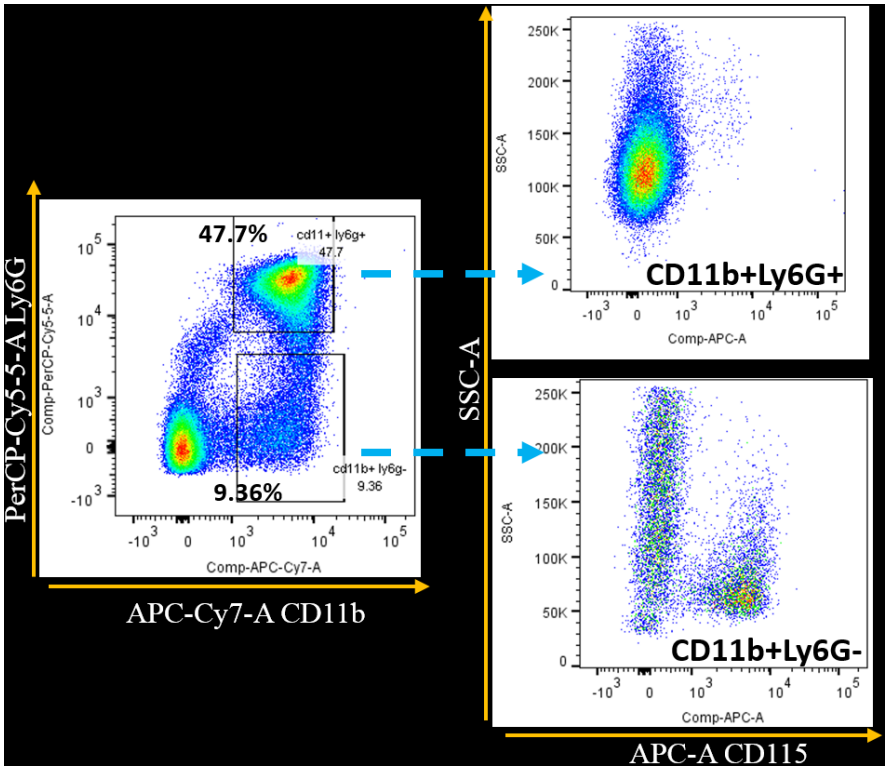

Figure.16: CD115+ cells percentages in CD11b+Ly6G+, and CD11b+Ly6G- splenocytes as analyzed by flow cytometry. Total mouse splenocytes from a tumor bearing BALB/c mouse was prepared as described in Materials and Methods. Debris (SSC-A vs. FSC-A) and doublets (FSC-H vs. FSC-A) were excluded. CD11b+ Ly6G+ cells and CD11b+ Ly6G- cells were gated out (Right) to check the level of CD115 in each subpopulation (Left) as pointed by blue dashed arrows. The majority of the CD115+ monocytes were found in CD11b+ Ly6G- subset. Frequencies of cells in each sub-gate (after doublet and debris elimination) are stated as a fraction of live cells.

Adoptive transfer of isolated monocytes. The CD115+ Ly5G- monocytes were then stained with Cell Proliferation dye eFluor® 450 (eBioscience) fluorescent dye and injected into HA++ mouse. After five days, we sacrificed the mouse, together with an un-injected control parental mouse to analyze tumors and spleens for the presence of donor monocytes/macrophages by FACS (**Figure.17**). We observed the presence of donor cells in both CD11b+F480+, and CD11b+ F480- subpopulations of myeloid cells present in the

tumor tissues, but not in the spleen. These data suggest that the monocytes (CD11b+ F480-) have migrated after the intravenous adoptive transfer to the tumor tissues, and some of them developed into macrophages (CD11b+F480+). This is also suggesting that the splenic donor monocytes have the tumor homing ability and could be used in our future experiments.

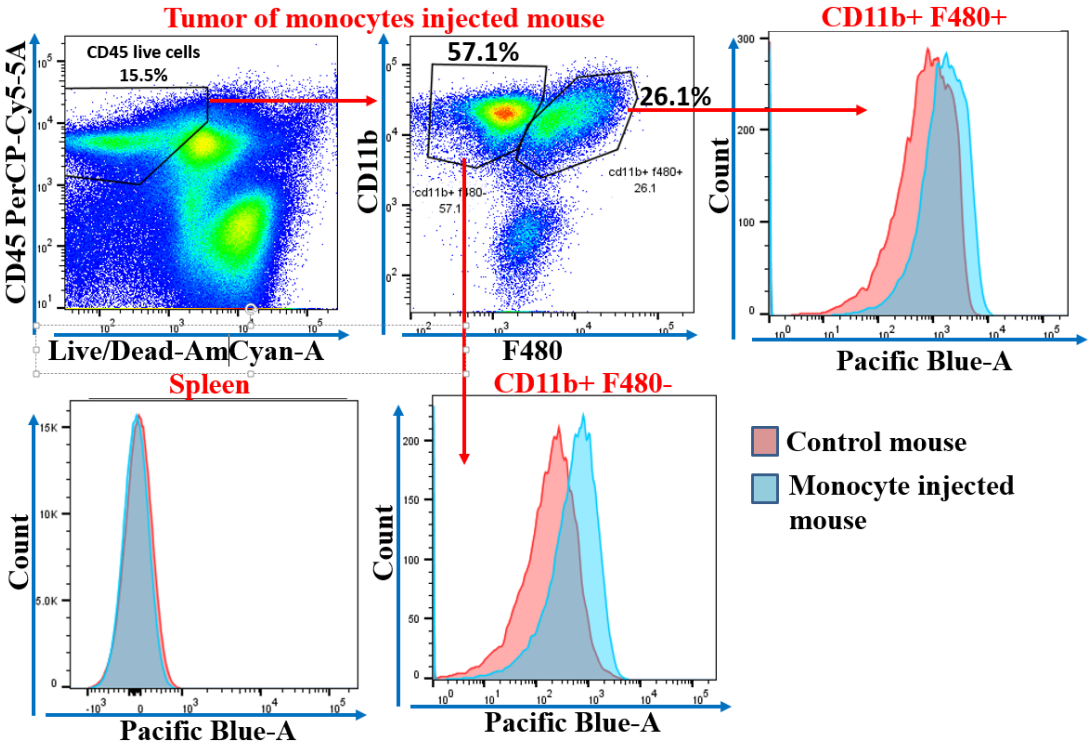

Figure.17: Flow cytometry analysis for the surface expression of CD11b, F480, and the labeled (pacific blue) donor monocytes within the CD45+ live cells. The cells in this analysis were recovered from tumor and spleen of the HA++ recipient mouse after adoptive transfer of labelled CD115+ monocytes, and an un-injected control parental mouse. The histograms for the pacific blue staining showed a positive signal in both CD11b+F480+, and CD11b+ F480- subsets in the HA++ tumor when compared with the control tumor. In the spleens from both tumors, there was no pacific blue signal. Debris (SSC-A vs. FSC-A) and doublets (FSC-H vs. FSC-A) were excluded. LIVE/DEAD® Fixable Aqua Dead Cell Stain was used to exclude the dead cells. The red arrows indicate the gating strategy used in the analysis.

V. Discussion

Immune evasion was recently recognized as one of the cancer hallmarks (28). One of the main mechanisms promoting immune evasion in cancer is the establishment of an immunosuppressive microenvironment. Our laboratory has developed a cell- and gene-based strategy for the tumor targeted delivery of a potent immunostimulatory molecule: IFN-α. This strategy strongly inhibited primary breast cancer and breast cancer lung metastasis by inhibiting tumor angiogenesis and promoting recruitment and activation of both innate and adaptive immune cells (74). Recently, silencing of type I interferons was shown to promote breast cancer metastasis by compromising an anti-tumor T cell response (22). For this reason, we are now proposing to test the efficacy of our IFN-α-delivery strategy in inhibiting breast cancer bone metastasis, one of the most lethal form of breast cancer.

Preclinical tumor models are an essential element of the tumor biology studies and for testing novel anti-tumor therapeutics (55). It is obviously emerging that with the intention of professionally asses a novel therapeutic approach and accelerate the clinical validation, preclinical tumor models should encompass most of the following: (i) reproduce the heterogeneity of cancer cell–stroma interactions in human disease; (ii) can be characterized at the molecular level, and harmonized with human disease; (iii) take into concern species-specific discrepancies; and (iv) link preclinical outcomes with desired clinical readout, e.g. tumor regression (75).

The variations in the level of genes expression (overexpression or deletion) were used to generate genetically engineered mouse models. The relevant genes to human tumorigenic process in each tumor type, are the most common to use. Few transgenic mouse models including two breast carcinoma mouse models of MMTV-PyMT (76) and the MMTV- Erbb2 (77) develop metastatic breast cancer to lungs, bones, brain, or liver. However these are

considered multistage carcinogenesis models, the repetitive surgical resection of the multiple asynchronously arising primary tumors in such mice is not practical or challenging which strictly restrict reproducing typical clinical conditions. The possibility of advanced multiple metastases, and distant metastatic spread could be acquired at several distant organs by orthotopic transplantation of late stage primary tumor cells, especially if the primary tumors were surgically resected (11). This allows sufficient time and prolongs survival for disseminated cells from the primary tumor to grow into established metastases, thus reconstructing the multiple consecutive steps that are accompanying with the metastatic cascade.

We now propose to investigate the efficacy of murine Tie2-IFN-α delivery platforms in a relevant preclinical model of spontaneous and experimental breast cancer metastasis targeting both lungs and bones: the 4T1.2 mouse model. The 4T1.2 subclone (58) has an increased frequency of bone metastasis after inoculation into the mammary fat pad (for spontaneous metastasis) or left ventricle of the heart (for experimental metastasis) when compared with the parental 4T1 cell line. In the experimental metastasis model, tumor cell distribution is synchronized by the intracardiac injection which dropping variability and thus permitting us to accomplish efficacy studies in the absence of confusing effects on the primary tumor.

Histological examination at the end point of treatment for quantification of lung and bone metastasis is difficult and time consuming. Moreover, significant information on the treatment response over time might be confused or missed by only examining the end point tumor burden, such as regression versus partial relapse. Therefore, the longitudinal assessment of tumor and metastatic burden during tumor progression and therapeutic intervention by developing novel preclinical models are fundamental to test new therapies. This is particularly critical in the case of bone and lung metastasis, whose volume

(increase/decrease) cannot be measured using a caliper as in subcutaneous mammary primary tumors.

Aim1. Tumor cell lines that can be traced *in vivo* during tumorigenesis and metastasis provide vital tools for investigating therapeutic responses (74). Bioluminescence imaging (BLI) and fluorescence are noninvasive imaging tools that offer the capability to perform real-time sequential imaging to improve the evaluation for therapeutic treatment response and/or reflection of tumor progression (78). In addition, noninvasive imaging lets researchers to use less animals with better statistical significance.

We used orthotopic implantation of murine mammary adenocarcinoma cancer cells 4T1.2 which are stably expressing the intracellular Fluc. This allows longitudinal imaging of tumor progression using whole-body bioluminescence in the presence or absence of an intact primary tumor. However, preliminary data in our laboratory had shown discrepancy between *in vivo* tumor growth of 4T1.2 cells and BLI signal, especially in larger tumors and lung metastasis which were often negative for the BLI. For this reason and in order to develop a new non-invasive method for the longitudinal quantification of metastatic burden, we explored the use of secreted Gluc that can be easily detected in the blood of mice injected with $sGLuc^{+}$ tumor cells (79). Towards this goal, lentiviral transduction with a vector encoding for the sGluc and the CFP reporter gene was performed into 4T1.2 cells that already express the Fluc and the mCherry protein (**Figure.4A**).

sGluc analysis. Our *in vitro* data show that 4T1.2 cells can be efficiently transduced to express sGluc and release it in the tissue culture medium. Moreover, its expression does not change the *in vivo* growth rate of the transduced cells when compared to the non-transduced parental cells. However, the sGluc signal is quickly decreasing in the circulation *in vivo*. 4T1.2 cells were injected into immunocompetent mice, therefore, an immunogenic response against a non-self-protein were observed (64, 79). However, further investigation is required

to distinguish between counter selection of sGluc expressing cells, vector silencing or production of anti-Gluc antibodies.

Additional problems were observed with respect to the co-expression of the Fluc and mCherry genes. *In vitro* culture of cells sorted for high levels of mCherry (HA++) resulted in loss of mCherry expression (**Figure.4D** and **Figure.5**) but not of Fluc expression as measured by BLI in their cell extracts (**Figure.7**). More importantly, cells that were selected as mCherry negative (HA+), indeed expressed high levels of Fluc (**Figure.7**). These data suggest that the mCherry cassette is easily silenced *in vitro* and cannot be used as a reporter gene for the co-expression of Fluc. These results were further confirmed *in vivo* where the Fluc and mCherry signals were rarely co-localising (**Figure.10B**). This inconsistent co-expression agreed with some recent studies that reported possible cryptic transcripts activity within the Fluc coding region (63) which might explain our results.

Fluc analysis. *In vivo*, the Fluc and mCherry signals were used for localization and quantification of growing tumors (**Figure.10**). In agreement with preliminary data from our laboratory, the Fluc signals were not always correlated with the presence and growth of primary and especially metastatic tumors. More often mice with heavy tumor metastatic burden, as shown by post-mortem examination, did not have any Fluc signal in the lungs or bones (**Figure.10**C). Similarly, no consistent correlation was found between primary tumor growth and Fluc signal. Only few tumors were and remained positive for Fluc and had a signal that was increasing with tumor growth. Other tumors never showed any signal, and some lost the signal (**Figure.10A, E**).

The *in vivo* mCherry fluorescent assays had a much higher background than the BLI assay. Such a high background obscured or lowered the actual signal, even when using specific optical filters, which are, however, not ideal to discriminate between excitation and emission wavelengths. Also, it was not clear if the presence of CFP fluorescent protein could interfere

with the mCherry signal and contributed to the observed background. This was not the case in the Fluc bioluminescence assay that did not require photons for the excitation, and therefore Fluc did not establish a strong background. Moreover, the *in vivo* results with inconsistent Fluc signals in tumors and metastasis as well as the decreasing sGluc signals in the blood require further investigation to discriminate between counter-selection of expressing cells versus partial or complete silencing of the vectors.

Fluorescence is practically indicated for analysis via fluorescent microscopy (80) and flow cytometry. We will, therefore, test the presence of CFP protein (the reporter for sGluc) and mCherry (the reporter for Fluc) in the primary tumor tissue and metastatic organs. Anti-HA tag antibodies can also be used to monitor the expression of sGluc by western blot analysis on tissue extracts or immunostaining on tissue sections. If the CFP protein and the HA tag are expressed in HA+, and HA++ tumors or metastasis, it would suggest that anti-Gluc antibodies production and not counter selection against the sGluc+ cells or silencing of the vector has happened. Similarly, the presence/absence of mCherry will help understanding the inconsistency between mCherry and Fluc signals. Another option is the *ex vivo* quantification of the metastatic burden in the collected organs by qPCR for the mCherry DNA in lungs and bones. The presence of mCherry DNA in the absence of mCherry and/or Fluc signals would strongly suggest silencing of the vector.

Bone metastases. Although the bone metastases may be established anywhere in the skeletal system, the majority of lesions occur in the axial skeleton. In human, it commonly affect the vertebrae, proximal parts of the femur or humerus, pelvis, ribs, and skull (81).

Bone metastases lesions can be of many different types that vary according to the type of cancer, location and developmental stages. In breast cancer they are known to be mainly

osteolytic. Other types of bone metastasis can be sclerotic or mixed lesions, depending on the relationship between the osteoblastic and osteoclastic remodeling progressions. Lesions in the medullary cavity, extend to medullary bone, and then the cortex (82). The sclerotic rim of affected bone is an initial indicator of osteolytic lesion healing, that grow and develops from periphery to the lesion center, making the lesion shrink and resolve (81) (**Figure.11**). This development therefore could help monitoring healing response to assess therapeutic efficacy. For example, increasing osteolysis indicates disease progression, while a uniform lesional sclerosis shows healing. We could not identify these different developmental stages because only a very low number of mice were showing bone lesions, and we killed the mice once this affect the mice movement at very early stages.

Radiographic imaging could be used for a possible diagnosis of bone metastases. However, if bone metastases are assumed or existing, further imaging-guided techniques such as MRI, or CT scans should be done to approve the diagnosis, and understand the disease extent. This is important because radiographs are somewhat insensitive to recognize small or early metastatic foci. However, CT scanning has limited skeletal coverage, and is also insensitive for small intramedullary lesions (83).

Radiography is relatively insensitive in detecting bone metastases, especially subtle lesions without cortical involvement, and advanced cancellous bone destructive lesions. Generally, only lesions larger than 2 cm in human are radiographically visible, and after 50% loss of bone mineral content (84). Moreover, osteolytic metastases can mimic spine Schmorl nodes and subchondral cysts that make the diagnosis much difficult. Also, osteolytic lesions could look similar to cystic angiomatosis, amyloidosis, and infiltrative bone marrow lesions (81). For these reasons, MRI bone scintiscans is considered the best imaging strategy to detect metastatic lesions before changes in bone metabolism (84), although expensive and not widely available.

The number of mice that showed metastasis in lungs and bones were relatively low for both HA and parental 4T1.2 cells. This happened because the primary tumor developed rapidly to large size (>1cm^2) and extended into the peritoneum and sometimes internal organs, which made the excision the primary tumor by surgical laparotomy difficult, and many mice were euthanized post-surgery for ethical reasons, thus compromising long-term analysis of metastasis development.

For the analysis of spontaneous metastasis we need to optimize time of primary tumor resection and mice recovery post-surgery. We will also set up and optimize intracardiac injection of 4T1 and/or 4T1.2 cells to obtain lung and bone experimental metastasis in the same mouse. To optimize this, we need to identify the number of cells to inject, and the time of metastasis development. *In vivo* monitoring of bone metastasis will be further improved by comparing PET-CT imaging versus X-ray for *in vivo* localization and follow up.

The bone resorbing cytokines such as PTHrP (58), IL-6 (85) and IL-11 (86), and also the calcium levels in bones (58) were found to contribute in enhancement for the metastasis to the bone. The release of these cytokines as well as changes in the levels of calcium can be easily monitored in the blood of tumor bearing mice. Therefore, their measurements in the blood of 4T1.2 tumor bearing mice versus wildtype mice and mice injected with non-metastatic breast cell lines such as 66cl4 or 67NR could be a good indicator for bone metastasis development.

Aim2. Autologous transplantation of HSCs is not always an option, moreover insertional mutagenesis associated with vector integration and stable engraftment of HSCs might represent a long-term risk. For this reason we are testing whether adoptive transfer of mature

engineered monocytes could be used as an alternative to HSCs transplantation for the delivery of IFN-α,

One of the first steps in developing this new strategy is the identification of an experimental source of mature mouse monocyte that would provide us with a sufficient number of cells to inject several recipient mice in our experiments. Towards this goal we identified spleen of tumor bearing mice as a promising source of murine monocytes.

Splenic monocytes. The main functions of spleen are to eliminate the aged RBCs for iron recycling, provoke the immune system, and provide the RBCs in emergency (87). Whereas DCs and macrophages are mainly sessile as a tissue-resident cells, the monocytes are considered blood circulating cells (88).

Splenic monocyte populations included Ly-6C^{hi} and Ly-6C^{low} subtypes in similar ratios to the circulating monocytes (89). While the main role of Ly6C^{low} monocytes is to recruit neutrophils to maintain and repair the blood vessel endothelial surface, Ly6C^{hi} monocytes are quickly recruited by extravasation into sites of tissue remodeling and inflammation, where they differentiate into monocyte-derived macrophages and monocyte-derived DCs (90). Monocytes express CD115 and CD11b (**Figure.16**) and are low or negative for Ly-6G, CD90, NK1.1, B220, and CD49b surface markers. They can be easily distinguished from DCs and macrophages in terms of the CD11c, F4/80 glycoprotein, and MHC I expression. The spleen could be a great compartmental storage of extramedullary monocytes that increased in number in response to stress stimuli such as during wound healing (89) or tumor progression.

The splenic monocytes are distinguishable from tissue-resident macrophages and contribute in inflammatory responses (91). Because blood monocytes resembled their splenic counterparts morphologically in terms of cell size and nucleus shape, as well as functionally

in terms of phagocytic activity, differentiation potency, transcriptomes, and protein analysis (89), we are currently optimizing a purification protocol for the isolation and characterization of CD11b+Ly6G−CD115+ splenic monocyte as potential candidate for our adoptive transfer strategy.

Because in tumor-bearing mice the myeloid compartment is increasing markedly with a decrease in erythroid and lymphoid populations (71), we analyzed the blood, bone marrow and spleens for the presence, percentage and absolute numbers of CD115+ monocytes and identified spleens as the most abundant source of monocytes.

Sorting problems with CD115+ cells. Single antibody is not sufficient for splenic monocytes and macrophages demarcation, because of the distinct splenic myeloid compartment that contains eosinophils, neutrophils, and dendritic cells which share common expression patterns for myeloid specific antigens (92). Based on the surface expression of CD11b, CD115 and Ly6G, we designed a purification protocol consisting in a Ly6G+ cell depletion step followed by sorting of CD115+ cells (**Figure.14** and **Figure.15**), Unexpectedly, we could not sort a significant number of CD115+ monocytes to be injected into tumor bearing mice. We still need to investigate whether this happens because of monocyte activation resulting in CD115 receptor downregulation or internalization, or a technical problem with the MACS step. CD115 is still our ideal marker in terms of monocytes specificity, however, recent reports described similar problems in using CD115 for isolation purposes, with a 33% decline in CD115 expression in monocytes after storing at room temperature for 0 to 4 hours. To maintain CD115 stable expression on the cell surface, researchers recommended to treat samples with EDTA and store them at a low temperature before processing (93).

As an alternative, we are considering to combine a depletion step in which we deplete most lineages using a cocktail of lineage-specific antibodies including antibodies targeting T, B

and NK cells as well as granulocytes, followed by a sorting of the remaining CD11b+ cells. These remaining CD11b+ cell will be strongly enriched in monocytes. This protocol will avoid the use of CD115 as a purification marker.

CD11b is expressed by different cells such as activated T cells, NK cells, myeloid cells, and B cells (94-96). According to Rose et al. (92) a panel consisting of mPDCA-1, CD11b, CD11c, Ly6C, Ly6G, B220, and NK1.1 could be the best solution to sort out the mouse splenic monocytes whose purity could be confirmed by some other restricted markers like Siglec F, CD115, and MHC Class II.

Another option is to use a transgenic animal with a genetic knock-in to fluorescent protein gene that should allow monitoring leukocyte trafficking and recruitment (97). By using the CD68-GFP mice that express high-level GFP reporter gene in monocytes of blood, bone marrow, and spleen, we can track the monocyte and macrophages trafficking, recruitment and differentiation *in vivo* to the tumor tissues (98).

Other monocytes delivery routes. Recent publications have shown that macrophages injected systemically are pooled in the liver and spleen after being retained in the lungs firstly, and then eventually move to metastatic locations, while macrophages delivered intraperitoneally persisted in the peritoneal cavity for a week before accumulating within rapidly growing tumors (99). Thus, to improve the outcome of our therapy by reducing monocytes accumulation in healthy tissues and increasing their accumulation in tumors, it might be necessary to test alternative monocytes administration routes other than the intravenous injection such as intratumoral, intratracheal, and osteal administrations, depending on the type of tumor and metastasis. Careful analysis of the biodistribution, invasive nature, therapeutic potential, circulation kinetics, accessibility, and dosage-limiting toxicities in tumor and healthy surrounding tissues will be required. Moreover, the

combination of two or more approaches may have substantial effect for further improving our anticancer therapy.

Monocytes alternatives. As an alternative to monocytes, we will consider isolation/generation of macrophages. Both bone marrow and blood derived macrophages can be efficiently generated *in vitro* from myeloid precursor of the bone marrow or circulating monocytes.

The monocytes are limited in the blood, and show antitumor response and may be potentially beneficial for adoptive cellular immunotherapy (100). However it was reported recently that monocytes can be derived from the human venous blood and expanded *in vitro* by using modified Rosewell Park Memorial Institute medium (RPMI)-1640 that supplemented with 10% non-inactivated autologous serum and avian feeder cells (101).

It was reported that the number of the monocytes in blood increased by two to fourfold upon injection of recombinant human GM-CSF (rhuGM-CSF). After *in vitro* overnight incubation with IFN-ɣ, the mobilized monocytes differentiated into macrophages with no treatment related toxicities, and high phagocytic and cytotoxicity profiles (102). In another study, the peritoneal macrophages were collected after thioglycollate induced inflammation. To sensitize the macrophages to the tumor, they were cultured *in vitro* with lymphocytes and tumor supernatants. Upon administration *in vivo*, the macrophages were highly active in preventing pulmonary metastases, while those exposed only to tumor supernatants were not functional (103). Those studies and others (104, 105) proves the macrophages feasibility and safety in adoptive transfer for tumor inhibition.

The protocols described above mainly generate pro-inflammatory M1-like macrophages characterized by an anti-tumoral activity. Although after injection into tumor bearing mice, the tumor might polarized the macrophages phenotype more towards an M2-like phenotype.

We know that M1 macrophages do not express Tie2 (106) and therefore they would not express and deliver IFN-α. *In vitro* treatments with different combinations of cytokines such as TNF, IL4, and IL6 (103) will be explored for the generation of more M2-like macrophages.

Future directions.

Enriched characterization and understanding of the leading genetic modifications and different molecular subtypes of breast cancer and signaling pathways have identified several novel targets that will enable the health care providers to give each patient the appropriate therapy (7). Targets such as angiogenesis inhibitors, intracellular signaling inhibitors, tyrosine kinase inhibitors, rapamycin analogs, poly (ADP-ribose) polymerase inhibitors, and DNA repair inhibitors have revealed outstanding clinical efficacy (107-109), and some of these agents are studied owing to initial clinical trials response. Unfortunately, many therapeutic strategies are associated with development of resistance, relapse of the primary tumor and/or dissemination and growth of treatment resistant metastasis. Many of these evasive mechanisms are mediated by responses with in the tumor microenvironment like for example increased recruitment of pro-angiogenic and immunosuppressive bone marrow derived myeloid cells upon anti-angiogenic therapy.

Here, we are suggesting different directions to develop more effective anti-tumor therapies. We are using a component of the tumor microenvironment as a vehicle to deliver an anti-tumoral biomolecule that is mainly targeting the tumor microenvironment by rendering it less permissive for the tumor cells. For this purpose we used tumor infiltrating Tie2-expressing monocytes/macrophages for the delivery of IFN-α.

More recently, we developed a human IFN-α delivery platform and a preclinical model in human hematochimeric mice to test the efficacy of our strategy on human breast cancer

tumors in the presence of a human hematopoietic system. Together, these results indicated development of a functional human immune system within the mouse that can reject allogeneic human tumor, but only after reversion of the immunosuppressive microenvironment mediated by the tumor targeted delivery of IFN-α (45, 46).

Mesenchymal stem cells and humanized models. By applying the same strategy, human hematochimeric NSG mice will be challenged with MDA-MB-231 variants that show different organ tropism (62, 110), upon intravenous versus intracardiac injection. Luciferase expressing variants are also available to us (111) for bioluminescent analysis of *in vivo* tumor localization, progression and quantification. This humanized model will be further explored in collaboration with the laboratory of Prof. D. Hutmacher (QUT) who recently developed a technique to engineer human-derived bone in immunodeficient mice, which can be applied to mimic human-specific mechanisms of bone metastatic disease (112, 113). Injection of breast cancer cells into the bloodstream of these mice leads to the development of bone-destructive metastases in the humanized bone implants that closely reproduce clinical bone lesions in breast cancer patients (114).

The bone marrow (BM) environment encompasses different types of non-hematopoietic cells such as chondrocytes, osteocytes, adipocytes, and fibroblasts. Despite human genetically modified HSCs can be transplanted into immunocompromised mice, the engraftment and multilineage reconstitution of human cells are suboptimal due to lack of a human BM niche. Thus, the subcutaneous implantation of humanized bone generated using human MSCs might provide the missing environment for an efficient engraftment oh human HSCs (115). Human MSCs can work as precursors of various subsets of BM non-hematopoietic cells (116), and accordingly generating scaffolds with stem cell niches similar to human HSC niches in terms of self-renewal, differentiation, and proliferation capacities. This would imitate the *in vivo* physiological positive and negative regulatory aspects (117). For these reasons, we

hypothesize that using this *vivo* extramedullary bone model in NOD/SCID/IL-2rɣ null mice (116) can be helpful to test our therapy efficacy in bone metastasis.

The ability of the MSCs to differentiate into pericytes and endothelial precursors through the PDGF-B-NRP-1 signaling pathway is a challenge because this might help to improve the tumor angiogenesis (118). Also the MSCs ability to inactivate T-cell functions for inducing immunoregulatory effects and control the tissue damage (119) can be a great challenge for our therapy that aims to activate the immune system.

Using the MDSCs as a blood indicator for bone metastasis. It was recently shown that Ly6G^{hi} CD11b+ MDSCs are more abundant in the bone marrow of mice carrying 4T1.2 bone metastasis models than in the primary tumors or metastatic lungs in the same animals, or the corresponding organs in the native mice. Those cells act against the tumor immunosurveillance through inhibition of CD4+ and CD8+ T lymphocytes proliferation. However, the forced expression of IRF7 in 4T1.2 cells enhanced the IFN pathway that directly stimulate the T cell and NK cell effector proliferation and prevented the expansion of Ly6G^{hi} CD11b+ MDSCs probably by inhibiting the expression of G-CSF a cytokine known to promote expansion and mobilization of MDSCs (22). Therefore the MDSCs levels could be used as an indicator for the efficacy of our IFNα therapy.

Combining therapies. Individual agent therapies that targeted tumor vasculature rarely results in the eradication of tumors, despite efficient inhibition of tumor growth in preclinical mouse models. Drug combinations in the past were alleged to be more toxic and not practical than monotherapy. However, recently it became clear that the sequential application and combination of different treatments is more effective in metastatic breast cancer patients due to the ability to target tumor cells heterogeneity. For example, different types of immunotherapies such as adoptive cellular therapy, cytokine therapy, and vaccines as well as radiotherapy and chemotherapy could be is used in combinations with more conventional

chemotherapy (120). Recent gene profiling studies showed that metastatic breast cancer cells are transitional in their gene expression levels form stem cell and epithelial-to-mesenchymal transition-associated genes in low-metastatic burden tumors, toward luminal differentiation-associated genes in high-metastatic burden tissues to look similar to the heterogeneous primary tumor cells (121). This would suggest that when developing new therapies, not only the type of combinations and cancer heterogeneity are important, but also the tumor cells hierarchical progression is essential to decide proper time for intervention.

1. Check point inhibitors. Among the different types of immunotherapies, monoclonal antibodies directed against immune checkpoint molecules are of particular interest. Antibodies against inhibitory checkpoint molecules, for instance, can bind and block the T cell regulatory pathways. Antibodies against the cytotoxic T lymphocyte antigen 4 (CTLA-4), programmed cell death protein 1 (PD-1) and programmed cell death 1 ligand 1 (PD-L1) inhibitors promote T cell activation, and decrease the levels of intratumoral Tregs (120). Therefore, monoclonal antibodies against inhibitory checkpoint molecules and IFNs have diverse synergistic mechanisms which could overcome the immunosuppressive microenvironment and initiate strong favorable clinical impacts, especially in case of CNS metastases because activated T cells can traffick to the brain, even though antibodies cannot cross the blood–brain barrier (122).

2. Type II interferons. Unlike type I interferons that targeted host hematopoietic cells, IFN-gamma only targets the tumor cells. Therefore, type II interferons does not entirely overlap the functions of IFN-alpha/beta. In contrast to the IFNGR1 (IFN type II receptor) deficient sarcomas that were rejected only upon IFNGR1 re-establishment, the IFNAR1 knocked out sarcomas (insensitive to type I IFN) were rejected upon injection into naive wild-type syngeneic mice and was not converted into regressor tumors after expression of IFNAR1 was restored. On the other hand, the sarcoma cells derived from IFNAR1 and IFNGR1 knockout

mice (insensitive to both type I and II IFN) were rejected only by restoring the IFNγ sensitivity, but not type I IFNs. Moreover, IFNAR1 knockout mice could not react against the transplanted tumors except after being lethally irradiated and transplanted with wild-type bone marrow (123). These findings clarify that the immunogenicity of tumor cells is controlled by IFNγ, but not type I IFN, and therefore Type II interferons might be helpful in a combination therapy.

3. RANK and RANKL. Receptor Activator of Nuclear Factor κ B (RANK) and its ligand (RANKL) are potent inducer of osteoclast formation and normal breast lobuloalveolar structures development in pregnancy. However, RANKL-RANK interaction was found to enhance mammary tumor development (20). Therefore, we hypothesize that a combination of our IFN-α targeted therapy and RANKL monoclonal antibody can inhibit the osteoclast and improve the immune function simultaneously.

4. Use the CSF1 for the monocytes pretreatment. The human CD14+ monocytes pre-treatment with Macrophage Colony-Stimulating Factor (CSF1) give rise to the Tie2 receptor expression and TEMs migratory ability. Culturing the human umbilical vein endothelial cells (HUVECs) with conditioned supernatants from these TEMs resulted in a substantial increase in branch points. Anti-CSF1R and Tie2 receptor knockdown on monocytes abolished the CSF1 and ANG2 synergistic effect (124). Therefore, we can propose that treating the IFN-α transduced monocytes with CSF1 will help their recruitment to tumor tissues and enhance their productivity. On the other end, expression of IFN-α might counteract their protumoral activity induced by CSF1.

VI. Conclusion

Breast cancer has important economic and social drawbacks, with significant deaths among the Australian women. The up-regulation of the TIE2 promoter expression in TEMs upon homing to tumor tissue enabled us to increase IFN-α local targeted delivery to tumor tissues in distant organs such as bones and lungs, with low systemic levels to overcome the significant systemic toxicity of IFN-α (51, 125). This strategy is aimed to enhance the immune responses against the metastatic breast cancer by successfully reprogramming the tumor microenvironment to counter its immune evasive feature. Both permanent engraftment of engineered HSCs that continuously supply new monocytes progeny, as well as adoptive transfer of mature engineered monocyte have been considered in this project.

Utilizing a clinically pertinent *in vivo* model of breast cancer metastasis to bones was not only valuable for metastatic burden quantification but it is also of huge significance in defining the correlation with other diagnostic tools. This has not been likely previously, and may be in charge for the shortage of molecular markers as prognostic indicators for immunotherapies and targeted therapies efficacy. In this study we are testing the use of an immunocompetent *in vivo* model of spontaneous breast cancer metastasis to bones and lungs with the adoptively transferred adult monocytes. Adoptive transfer of autologous immune cells permits the interaction between a compatible and functional immune system and the tumor cells within the tumor microenvironment. Such an interaction is known to be fundamental in the modulation of tumor development and progression.

We expect that sustained research will confirm the clinical convenience of tumor targeted IFN-α cellular therapy, setting the platform for eventual FDA approval. Furthermore, clinical trials combining this therapy with other immunotherapies like checkpoint inhibitors will revive fruition, allowing innovative succeeding combination strategies.

VII. Acknowledgments

I am grateful to Dr. Roberta Mazzieri for supervision and critical comments during this project; Davide Moi for helpful discussions and assist in the *in vivo* experiments; Dr. Orla Gannon for help with molecular studies; Ryan Glea for vector production; and Nathan Boase for assistance with preclinical imaging. This research was supported by AusAid master awards (AAA).

VIII. References

1. DeSantis C, Siegel R, Bandi P, Jemal A. Breast cancer statistics, 2011. CA: A Cancer Journal for Clinicians. 2011;61(6):409-18.

2. Davis C, Williams P, Parle M, Redman S, Turner J. Assessing the Support Needs of Women With Early Breast Cancer in Australia. Cancer nursing. 2004;27(2):169-74.

3. Reis JS, Pusztai L. Breast Cancer 2 Gene expression profiling in breast cancer: classification, prognostication, and prediction. Lancet. 2011;378(9805):1812-23.

4. Weigelt B, Baehner FL, Reis-Filho JS. The contribution of gene expression profiling to breast cancer classification, prognostication and prediction: A retrospective of the last decade. Journal of Pathology. 2010;220(2):263-80.

5. Weigelt B, Horlings HM, Kreike B, Hayes MM, Hauptmann M, Wessels LFA, et al. Refinement of breast cancer classification by molecular characterization of histological special types. The Journal of pathology. 2008;216(2):141-50.

6. McArthur HL, Hudis CA. Breast cancer chemotherapy. Cancer Journal. 2007;13(3):141-7.

7. Bourdeanu L, Liu EA. Systemic treatment for breast cancer: chemotherapy and biotherapy agents. Seminars in oncology nursing. 2015;31(2):156-62.

8. Green JR. Antitumor effects of bisphosphonates. Cancer. 2003;97(S3):840-7.

9. Moorthi C, Manavalan R, Kathiresan K. Nanotherapeutics to overcome conventional cancer chemotherapy limitations. Journal of Pharmacy and Pharmaceutical Sciences. 2011;14(1):67-77.

10. Nguyen DX, Massague J. Genetic determinants of cancer metastasis. Nat Rev Genet. 2007;8(5):341-52.

11. O'Reilly MS, Holmgren L, Shing Y, Chen C, Rosenthal RA, Moses M, et al. Angiostatin: A novel angiogenesis inhibitor that mediates the suppression of metastases by a lewis lung carcinoma. Cell. 1994;79(2):315-28.

12. Pockaj BA, Wasif N, Dueck AC, Wigle DA, Boughey JC, Degnim AC, et al. Metastasectomy and Surgical Resection of the Primary Tumor in Patients With Stage IV Breast Cancer. ANNALS OF SURGICAL ONCOLOGY. 2010;17(9):2419-26.

13. Samiee S, Berardi P, Bouganim N, Vandermeer L, Arnaout A, Dent S, et al. Excision of the primary tumour in patients with metastatic breast cancer: A clinical dilemma. Current Oncology. 2012;19(4):e270-e9.

14. Rashid OM, Takabe K. Does Removal of the Primary Tumor in Metastatic Breast Cancer Improve Survival? Journal of Women's Health. 2014;23(2):184-8.

15. Weber GF. Molecular mechanisms of metastasis. Cancer letters. 2008;270(2):181-90.

16. Scully OJ, Bay B-H, Yip G, Yu Y. Breast cancer metastasis. Cancer Genomics and Proteomics. 2012;9(5):311-20.

17. Hunter KW, Crawford NPS, Alsarraj J. Mechanisms of metastasis. Breast Cancer Research. 2008;10(1):S2-S.

18. Roodman GD. Genes associate with abnormal bone cell activity in bone metastasis. Cancer and metastasis reviews. 2012;31(3):569-78.

19. Guise TA, Kozlow WM, Heras-Herzig A, Padalecki SS, Yin JJ, Chirgwin JM. Molecular Mechanisms of Breast Cancer Metastases to Bone. Clinical Breast Cancer. 2005;5(2):S46-S53.

20. Khosla S. Minireview: The OPG/RANKL/RANK system. Endocrinology. 2001;142(12):5050-5.

21. Debies MT, Welch DR. Genetic Basis of Human Breast Cancer Metastasis. Journal of mammary gland biology and neoplasia. 2001;6(4):441-51.

22. Bidwell BN, Slaney CY, Withana NP, Forster S, Cao Y, Loi S, et al. Silencing of Irf7 pathways in breast cancer cells promotes bone metastasis through immune escape. Nature medicine. 2012;18(8):1224-31.

23. Schreiber RD, Dunn GP, Koebel CM. Interferons, immunity and cancer immunoediting. Nature Reviews Immunology. 2006;6(11):836-48.

24. Indraccolo S. Interferon-α as angiogenesis inhibitor: Learning from tumor models. Autoimmunity. 2010;43(3):244-7.

25. Laoui D, Movahedi K, van Overmeire E, van den Bossche J, Schouppe E, Mommer C, et al. Tumor-associated macrophages in breast cancer: Distinct subsets, distinct functions. International Journal of Developmental Biology. 2011;55(7-9):861-7.

26. Martinez FO, Helming L, Gordon S. Alternative activation of macrophages: An immunologic functional perspective. Annual Review of Immunology. 2009;27(1):451-83.

27. Mantovani A, Sica A, Sozzani S, Allavena P, Vecchi A, Locati M. The chemokine system in diverse forms of macrophage activation and polarization. Trends in Immunology. 2004;25(12):677-86.

28. Horne SD, Pollick SA, Heng HHQ. Evolutionary mechanism unifies the hallmarks of cancer. International Journal of Cancer. 2015;136(9):2012-21.

29. Umansky V, Sevko A. Tumor Microenvironment and Myeloid-Derived Suppressor Cells. Cancer Microenvironment. 2013;6(2):169-77.

30. Ostrand-Rosenberg S. Immune surveillance: a balance between protumor and antitumor immunity. Current Opinion in Genetics & Development. 2008;18(1):11-8.

31. Sica A, Larghi P, Mancino A, Rubino L, Porta C, Totaro MG, et al. Macrophage polarization in tumour progression. Seminars in Cancer Biology. 2008;18(5):349-55.

32. Gajewski TF. Failure at the Effector Phase: Immune Barriers at the Level of the Melanoma Tumor Microenvironment. Clinical Cancer Research. 2007;13(18):5256-61.

33. Fridlender ZG, Sun J, Kim S, Kapoor V, Cheng G, Ling L, et al. Polarization of Tumor-Associated Neutrophil Phenotype by TGF-β: “N1” versus “N2” TAN. Cancer Cell. 2009;16(3):183-94.

34. Priceman SJ. Targeting distinct tumor-infiltrating myeloid cells by inhibiting CSF-1 receptor in solid tumors: ProQuest Dissertations Publishing; 2009.

35. Luo Y, Zhou H, Krueger J, Kaplan C, Lee S-H, Dolman C, et al. Targeting tumor-associated macrophages as a novel strategy against breast cancer. Journal of Clinical Investigation. 2006;116(8):2132-41.

36. Lin EY, Nguyen AV, Russell RG, Pollard JW. Colony-stimulating factor 1 promotes progression of mammary tumors to malignancy. Journal of Experimental Medicine. 2001;193(6):727-39.

37. Movahedi K, Laoui D, Gysemans C, Baeten M, Stangé G, Van Bossche JD, et al. Different tumor microenvironments contain functionally distinct subsets of macrophages derived from Ly6C(high) monocytes. Cancer Research. 2010;70(14):5728-39.

38. Eubank TD, Roberts RD, Khan M, Curry JM, Nuovo GJ, Kuppusamy P, et al. Granulocyte macrophage colony-stimulating factor inhibits breast cancer growth and metastasis by invoking an anti-angiogenic program in tumor-educated macrophages. Cancer Research. 2009;69(5):2133-40.

39. Qian B, Deng Y, Im JH, Muschel RJ, Zou Y, Li J, et al. A distinct macrophage population mediates metastatic breast cancer cell extravasation, establishment and growth. PLoS ONE. 2009;4(8):e6562.

40. Kitamura T, Qian B-Z, Soong D, Cassetta L, Noy R, Sugano G, et al. CCL2-induced chemokine cascade promotes breast cancer metastasis by enhancing retention of metastasis-associated macrophages. The Journal of Experimental Medicine. 2015.

41. De Palma M, Mazzieri R, Politi LS, Pucci F, Zonari E, Sitia G, et al. Tumor-Targeted Interferon-α Delivery by Tie2-Expressing Monocytes Inhibits Tumor Growth and Metastasis. Cancer Cell. 2008;14(4):299-311.

42. Mazzieri R, Pucci F, Moi D, Zonari E, Ranghetti A, Berti A, et al. Targeting the ANG2/TIE2 Axis Inhibits Tumor Growth and Metastasis by Impairing Angiogenesis and Disabling Rebounds of Proangiogenic Myeloid Cells. Cancer Cell. 2011;19(4):512-26.

43. Hanahan D, Bergers G. Modes of resistance to anti-angiogenic therapy. Nature Reviews Cancer. 2008;8(8):592-603.

44. Gentner B, Visigalli I, Hiramatsu H, Lechman E, Ungari S, Giustacchini A, et al. Identification of hematopoietic stem cell-specific miRNAs enables gene therapy of globoid cell leukodystrophy. Science Translational Medicine. 2010;2(58):58ra84-58ra84.

45. Escobar G, Moi D, Ranghetti A, Ozkal-Baydin P, Squadrito ML, Kajaste-Rudnitski A, et al. Genetic Engineering of Hematopoiesis for Targeted IFN-alpha Delivery Inhibits Breast Cancer Progression. SCIENCE TRANSLATIONAL MEDICINE. 2014;6(217):217ra3.

46. Escobar G, Gentner B, Naldini L, Mazzieri R. Engineered tumor-infiltrating macrophages as gene delivery vehicles for interferon-alpha activates immunity and inhibits breast cancer progression. ONCOIMMUNOLOGY. 2014;3(4).

47. Stoiber D, Imai K, Hayakawa S, Negishi H, Taniguchi T, Yanai H, et al. Integration of interferon-α/β signalling to p53 responses in tumour suppression and antiviral defence. Nature. 2003;424(6948):516-23.

48. Gao Y, Yang W, Pan M, Scully E, Girardi M, Augenlicht LH, et al. γδ T cells provide an early source of interferon γ in tumor immunity. Journal of Experimental Medicine. 2003;198(3):433-42.

49. Ivashkiv LB, Donlin LT. Regulation of type I interferon responses. NATURE REVIEWS IMMUNOLOGY. 2014;14(1):36-49.

50. Sheehan KC, Lai KS, Dunn GP, Bruce AT, Diamond MS, Heutel JD, et al. Blocking monoclonal antibodies specific for mouse IFN-alpha/beta receptor subunit 1 (IFNAR-1) from mice immunized by in vivo hydrodynamic transfection. Journal of interferon & cytokine research : the official journal of the International Society for Interferon and Cytokine Research. 2006;26(11):804-19.

51. Kiladjian J-J, Mesa RA, Hoffman R. The renaissance of interferon therapy for the treatment of myeloid malignancies. Blood. 2011;117(18):4706-15.

52. Oliveira IC, Sciavolino PJ, Lee TH, Vilcek J. Downregulation of Interleukin 8 Gene Expression in Human Fibroblasts: Unique Mechanism of Transcriptional Inhibition by Interferon. Proceedings of the National Academy of Sciences of the United States of America. 1992;89(19):9049-53.

53. Singh RK, Gutman M, Bucana CD, Sanchez R, Llansa N, Fidler IJ. Interferons alpha and beta down-regulate the expression of basic fibroblast growth factor in human carcinomas. Proceedings of the National Academy of Sciences of the United States of America. 1995;92(10):4562-6.

54. Cukierman E. A Visual-Quantitative Analysis of Fibroblastic Stromagenesis in Breast Cancer Progression. Journal of mammary gland biology and neoplasia. 2004;9(4):311-24.

55. Kim JB, Stein R, O'Hare MJ. Tumour-Stromal Interactions in Breast Cancer: The Role of Stroma in Tumourigenesis. Tumor Biology. 2005;26(4):173-85.

56. Yu JL, Rak JW. Host microenvironment in breast cancer development - Inflammatory and immune cells in tumour angiogenesis and arteriogenesis. BREAST CANCER RESEARCH. 2003;5(2):83-8.

57. Eckhardt BL, Parker BS, Van Laar RK, Restall CM, Natoli AL, Tavaria MD, et al. Genomic analysis of a spontaneous model of breast cancer metastasis to bone reveals a role for the extracellular matrix. Molecular Cancer Research. 2005;3(1):1-13.

58. Lelekakis M, Moseley JM, Martin TJ, Hards D, Williams E, Ho P, et al. A novel orthotopic model of breast cancer metastasis to bone. Clinical & experimental metastasis. 1999;17(2):163-70.

59. Pulaski BA, Ostrand-Rosenberg S. Mouse 4T1 breast tumor model. Curr Protoc Immunol. 2001;Chapter 20:Unit 20 2.

60. Kaur P, Nagaraja GM, Zheng H, Gizachew D, Galukande M, Krishnan S, et al. A mouse model for triple-negative breast cancer tumor-initiating cells (TNBC-TICs) exhibits similar aggressive phenotype to the human disease. BMC cancer. 2012;12:120.

61. Pupa SM, Ménard S, Forti S, Tagliabue E. New insights into the role of extracellular matrix during tumor onset and progression. Journal of cellular physiology. 2002;192(3):259-67.

62. Kang Y, Siegel PM, Shu W, Drobnjak M, Kakonen SM, Cordón-Cardo C, et al. A multigenic program mediating breast cancer metastasis to bone. Cancer Cell. 2003;3(6):537-49.

63. Vopálenský V, Mašek T, Horváth O, Vicenová B, Mokrejš M, Pospíšek M. Firefly luciferase gene contains a cryptic promoter. RNA. 2008;14(9):1720-9.

64. Van Rijn S, Nilsson J, Noske DP, Peter Vandertop W, Tannous BA, Würdinger T, et al. Functional multiplex reporter assay using tagged Gaussia luciferase. Scientific Reports. 2013;3:1046.

65. Mostoslavsky G, Kotton DN, Fabian AJ, Gray JT, Lee J-S, Mulligan RC. Efficiency of transduction of highly purified murine hematopoietic stem cells by lentiviral and oncoretroviral vectors under conditions of minimal in vitro manipulation. Molecular Therapy. 2005;11(6):932-40.

66. Zeng L, Yang S, Wu C, Ye L, Lu Y. Effective transduction of primary mouse blood- and bone marrow-derived monocytes/macrophages by HIV-based defective lentiviral vectors. Journal of Virological Methods. 2006;134(1):66-73.

67. Zhu T. HIV-1 genotypes in peripheral blood monocytes. Journal of Leukocyte Biology. 2000;68(3):338-44.

68. Eisenblatter M, Ehrchen J, Varga G, Sunderkotter C, Heindel W, Roth J, et al. In vivo optical imaging of cellular inflammatory response in granuloma formation using fluorescence-labeled macrophages. J Nucl Med. 2009;50(10):1676-82.

69. Cell Proliferation Dye eFluor® 450: eBioscience, Inc; 2015. Available from: http://www.ebioscience.com/cell-proliferation-dye-efluor-450.htm.

70. Stripecke R, Del Carmen Villacres M, Skelton DC, Satake N, Halene S, Kohn DB. Immune response to green fluorescent protein: Implications for gene therapy. Gene Therapy. 1999;6(7):1305-12.

71. Huynh H, Zheng J, Umikawa M, Silvany R, Xie X-J, Wu CJ, et al. Components of the Hematopoietic Compartments in Tumor Stroma and Tumor-Bearing Mice. PLoS ONE. 2011;6(3):e18054.

72. Fluorescence activated cell sorting of live cells: Abcam plc; 2015 [cited 2015 4th September]. Available from: http://www.abcam.com/protocols/fluorescence-activated-cell-sorting-of-live-cells.

73. MACS® MicroBeads - the most trusted and proven: Miltenyi Biotec; 2015 [cited 2015 4th September]. Available from: http://www.miltenyibiotec.com/en/products-and-services/macs-cell-separation/macs-technology/microbeads_dp.aspx.

74. De Palma M, Mazzieri R, Politi LS, Pucci F, Zonari E, Sitia G, et al. Tumor-targeted interferon-alpha delivery by Tie2-expressing monocytes inhibits tumor growth and metastasis. Cancer Cell. 2008;14(4):299-311.

75. Ruggeri BA, Camp F, Miknyoczki S. Animal models of disease: pre-clinical animal models of cancer and their applications and utility in drug discovery. Biochemical pharmacology. 2014;87(1):150-61.

76. Guy CT, Cardiff RD, Muller WJ. Induction of mammary tumors by expression of polyomavirus middle T oncogene: a transgenic mouse model for metastatic disease. Mol Cell Biol. 1992;12(3):954-61.

77. Ursini-Siegel J, Schade B, Cardiff RD, Muller WJ. Insights from transgenic mouse models of ERBB2-induced breast cancer. Nat Rev Cancer. 2007;7(5):389-97.

78. Christensen J, Vonwil D, Shastri VP. Non-Invasive In Vivo Imaging and Quantification of Tumor Growth and Metastasis in Rats Using Cells Expressing Far-Red Fluorescence Protein. PloS one. 2015;10(7):e0132725.

79. Tannous BA. Gaussia luciferase reporter assay for monitoring biological processes in culture and in vivo. Nature Protocols. 2009;4(4):582-91.

80. Tsuji A, World S. Bioluminescence & chemiluminescence: progress and perspectives. Hackensack, N.J;Singapore;: World Scientific Pub. Co; 2005.

81. Peh WC, Muttarak M. Imaging in Bone Metastases 2013 [cited 2015 19 October]. Available from: http://emedicine.medscape.com/article/387840-overview#a2.

82. Petrut B, Trinkaus M, Simmons C, Clemons M. A primer of bone metastases management in breast cancer patients. CURRENT ONCOLOGY. 2008;15(Suppl 1):S50-S7.

83. Cook GJR, Fogelman I. The role of positron emission tomography in the management of bone metastases. Cancer. 2000;88(S12):2927-33.

84. Algra PR, Bloem JL, Tissing H, Falke TH, Arndt JW, Verboom LJ. Detection of vertebral metastases: comparison between MR imaging and bone scintigraphy. Radiographics. 1991;11(2):219-32.

85. Crichton MB, Nichols JE, Zhao Y, Bulun SE, Simpson ER. Expression of transcripts of interleukin-6 and related cytokines by human breast tumors, breast cancer cells, and adipose stromal cells. Molecular and Cellular Endocrinology. 1996;118(1):215-20.

86. Lacroix M, Siwek B, Marie PJ, Body JJ. Production and regulation of interleukin-11 by breast cancer cells. Cancer Lett. 1998;127(1-2):29-35.

87. Mebius RE, Kraal G. Structure and function of the spleen. Nat Rev Immunol. 2005;5(8):606-16.

88. Auffray C, Fogg D, Garfa M, Elain G, Join-Lambert O, Kayal S, et al. Monitoring of blood vessels and tissues by a population of monocytes with patrolling behavior. Science. 2007;317(5838):666-70.

89. Swirski FK, Nahrendorf M, Etzrodt M, Wildgruber M, Cortez-Retamozo V, Panizzi P, et al. Identification of splenic reservoir monocytes and their deployment to inflammatory sites. Science. 2009;325(5940):612-6.

90. Auffray C, Fogg D, Garfa M, Elain G, Join-Lambert O, Kayal S, et al. Monitoring of Blood Vessels and Tissues by a Population of Monocytes with Patrolling Behavior. Science. 2007;317(5838):666-70.

91. Swirski FK, Nahrendorf M, Etzrodt M, Wildgruber M, Cortez-Retamozo V, Panizzi P, et al. Identification of Splenic Reservoir Monocytes and Their Deployment to Inflammatory Sites. Science. 2009;325(5940):612-6.

92. Rose S, Misharin A, Perlman H. A novel Ly6C/Ly6G-based strategy to analyze the mouse splenic myeloid compartment. Cytometry Part A. 2012;81A(4):343-50.

93. Breslin WL, Strohacker K, Carpenter KC, Haviland DL, McFarlin BK. Mouse blood monocytes: Standardizing their identification and analysis using CD115. Journal of Immunological Methods. 2013;390(1–2):1-8.

94. Dembic Z, Schenck K, Bogen B. Dendritic Cells Purified from Myeloma are Primed with Tumor-Specific Antigen (Idiotype) and Activate CD4+T Cells. Proceedings of the National Academy of Sciences of the United States of America. 2000;97(6):2697-702.

95. Solovjov DA, Pluskota E, Plow EF. Distinct roles for the alpha and beta subunits in the functions of integrin alpha(M)beta(2). JOURNAL OF BIOLOGICAL CHEMISTRY. 2005;280(2):1336-45.

96. Zhang Y, McCormick LL, Desai SR, Wu C, Gilliam AC. Murine Sclerodermatous Graft-Versus-Host Disease, a Model for Human Scleroderma: Cutaneous Cytokines, Chemokines, and Immune Cell Activation. The Journal of Immunology. 2002;168(6):3088-98.

97. Jung S, Aliberti J, Graemmel P, Sunshine MJ, Kreutzberg GW, Sher A, et al. Analysis of fractalkine receptor CX(3)CR1 function by targeted deletion and green fluorescent protein reporter gene insertion. MOLECULAR AND CELLULAR BIOLOGY. 2000;20(11):4106-14.

98. Iqbal AJ, McNeill E, Kapellos TS, Regan-Komito D, Norman S, Burd S, et al. Human CD68 promoter GFP transgenic mice allow analysis of monocyte to macrophage differentiation in vivo. BLOOD. 2014;124(15):E33-E44.

99. Andreesen R, Hennemann B, Krause SW. Adoptive immunotherapy of cancer using monocyte-derived macrophages: rationale, current status, and perspectives. Journal of Leukocyte Biology. 1998;64(4):419-26.

100. Stec M, Baran J, Szatanek R, Mytar B, Lenart M, Czupryna A, et al. Properties of monocytes generated from haematopoietic CD34(+) stem cells from bone marrow of colon cancer patients. Cancer Immunol Immunother. 2013;62(4):705-13.

101. Kadoi K. An in vitro monocyte culture method and establishment of a human monocytic cell line (K63). Vet Ital. 2011;47(2):139-46.

102. Hennemann B, Rehm A, Kottke A, Meidenbauer N, Andreesen R. Adoptive immunotherapy with tumor-cytotoxic macrophages derived from recombinant human granulocyte-macrophage colony-stimulating factor (rhuGM-CSF) mobilized peripheral blood monocytes. Journal of immunotherapy (Hagerstown, Md : 1997). 1997;20(5):365-71.

103. Lawrence T, Hagemann T. Tumour-associated macrophages. New York: Springer Science+Business Media, LLC; 2012.

104. Hagemann T, Lawrence T, McNeish I, Charles KA, Kulbe H, Thompson RG, et al. "Re-educating" tumor-associated macrophages by targeting NF-kappaB. The Journal of experimental medicine U6 - ctx_ver=Z3988-2004&ctx_enc=info%3Aofi%2Fenc%3AUTF-

8&rfr_id=info:sid/summonserialssolutionscom&rft_val_fmt=info:ofi/fmt:kev:mtx:journal&rftgenre=article&rftatitle=%22Re-educating%22+tumor-associated+macrophages+by+targeting+NF-kappaB&rftjtitle=The+Journal+of+experimental+medicine&rftau=Hagemann%2C+Thorsten&rftau=Lawrence%2C+Toby&rftau=McNeish%2C+Iain&rftau=Charles%2C+Kellie+A&rftdate=2008-06-09&rfteissn=1540-9538&rftvolume=205&rftissue=6&rftspage=1261&rft_id=info:pmid/18490490&rftexternalDocID=18490490&paramdict=en-US U7 - Journal Article. 2008;205(6):1261.

105. Ben-Efraim S, Tak C, Romijn JC, Fieren MJ, Bonta IL. Therapeutical effect of activated human macrophages on a human tumor line growing in nude mice. Medical oncology (Northwood, London, England). 1994;11(1):7-12.

106. Garcia S, Krausz S, Ambarus CA, Fernandez BM, Hartkamp LM, van Es IE, et al. Tie2 Signaling Cooperates with TNF to Promote the Pro-Inflammatory Activation of Human Macrophages Independently of Macrophage Functional Phenotype. PLOS ONE. 2014;9(1):e82088.

107. Bachelot T, Romieu G, Campone M, Diéras V, Cropet C, Dalenc F, et al. Lapatinib plus capecitabine in patients with previously untreated brain metastases from HER2-positive metastatic breast cancer (LANDSCAPE): A single-group phase 2 study. The Lancet Oncology. 2013;14(1):64-71.

108. Metro G, Foglietta J, Russillo M, Stocchi L, Vidiri A, Giannarelli D, et al. Clinical outcome of patients with brain metastases from HER2-positive breast cancer treated with lapatinib and capecitabine. Annals of Oncology. 2011;22(3):625-30.

109. Niikura N, Saji S, Tokuda Y, Iwata H. Brain Metastases in Breast Cancer. Japanese journal of clinical oncology. 2014;44(12):1133-40.

110. Minn AJ, Kang YB, Serganova I, Gupta GP, Giri DD, Doubrovin M, et al. Distinct organ-specific metastatic potential of individual breast cancer cells and primary tumors. JOURNAL OF CLINICAL INVESTIGATION. 2005;115(1):44-55.

111. Jenkins DE, Hornig YS, Oei Y, Dusich J, Purchio T. Bioluminescent human breast cancer cell lines that permit rapid and sensitive in vivo detection of mammary tumors and multiple metastases in immune deficient mice. Breast cancer research : BCR. 2005;7(4):R444-54.

112. Holzapfel BM, Thibaudeau L, Hesami P, Taubenberger A, Holzapfel NP, Mayer-Wagner S, et al. Humanised xenograft models of bone metastasis revisited: novel insights into species-specific mechanisms of cancer cell osteotropism. Cancer and Metastasis Reviews. 2013;32(1):129-45.

113. Thibaudeau L, Quent VM, Holzapfel BM, Taubenberger AV, Straub M, Hutmacher DW. Mimicking breast cancer-induced bone metastasis in vivo: current transplantation models and advanced humanized strategies. Cancer and Metastasis Reviews. 2014;33(2):721-35.

114. Thibaudeau L, Taubenberger AV, Holzapfel BM, Quent VM, Fuehrmann T, Hesami P, et al. A tissue-engineered humanized xenograft model of human breast cancer metastasis to bone. DISEASE MODELS & MECHANISMS. 2014;7(2):299-309.

115. Blau O, Baldus CD, Hofmann W-K, Thiel G, Nolte F, Burmeister T, et al. Mesenchymal stromal cells of myelodysplastic syndrome and acute myeloid leukemia patients have distinct genetic abnormalities compared with leukemic blasts. Blood. 2011;118(20):5583-92.

116. Chen Y, Jacamo R, Shi Y-X, Wang R-Y, Battula VL, Konoplev S, et al. Human extramedullary bone marrow in mice: A novel in vivo model of genetically controlled hematopoietic microenvironment. Blood. 2012;119(21):4971-80.

117. Nichols JE, Cortiella J, Lee J, Niles JA, Cuddihy M, Wang S, et al. In vitro analog of human bone marrow from 3D scaffolds with biomimetic inverted colloidal crystal geometry. Biomaterials. 2009;30(6):1071-9.

118. Fakhrejahani E, Toi M. Tumor Angiogenesis: Pericytes and Maturation Are Not to Be Ignored. Journal of Oncology. 2012;2012

119. Zonta S, De Martino M, Bedino G, Piotti G, Rampino T, Gregorini M, et al. Which is the most suitable and effective route of administration for mesenchymal stem cell-based immunomodulation therapy in experimental kidney transplantation: endovenous or arterial? Transplantation proceedings. 2010;42(4):1336-40.

120. Page DB, Postow MA, Callahan MK, Allison JP, Wolchok JD. Immune Modulation in Cancer with Antibodies. Annual Review of Medicine. 2014;65(1):185-202.

121. Lawson DA, Bhakta NR, Kessenbrock K, Prummel K, Yu Y, Takai K, et al. Single-cell analysis reveals a stem-cell program in human metastatic breast cancer cells. Nature. 2015;526(7571):131-5.

122. Tarhini AA, Cherian J, Moschos SJ, Tawbi HA, Shuai Y, Gooding WE, et al. Safety and Efficacy of Combination Immunotherapy With Interferon Alfa-2b and Tremelimumab in Patients With Stage IV Melanoma. Journal of Clinical Oncology. 2012;30(3):322-8.

123. Dunn GP, White JM, Schreiber RD, Koebel CM, Sheehan KCF, Uppaluri R, et al. A critical function for type I interferons in cancer immunoediting. Nature immunology. 2005;6(7):722-9.

124. Forget MA, Voorhees JL, Cole SL, Dakhlallah D, Patterson IL, Gross AC, et al. Macrophage Colony-Stimulating Factor Augments Tie2-Expressing Monocyte Differentiation, Angiogenic Function, and Recruitment in a Mouse Model of Breast Cancer. PLOS ONE. 2014;9(6):e98623.

125. Anguille S, Lion E, Willemen Y, Van Tendeloo VFI, Berneman ZN, Smits ELJM. Interferon-[alpha] in acute myeloid leukemia: an old drug revisited. Leukemia. 2011;25(5):739.